ARTICLE

Cul4 ubiquitin ligase cofactor DCAF12 promotes neurotransmitter release and homeostatic plasticity

Lilian A. Patrón[1,2], Kei Nagatomo[1], David Tyler Eves[1], Mays Imad[1], Kimberly Young[1], Meaghan Torvund[1,2], Xiufang Guo[1], Gregory C. Rogers[3,4], and Konrad E. Zinsmaier[1,3]

We genetically characterized the synaptic role of the *Drosophila* homologue of human DCAF12, a putative cofactor of Cullin4 (Cul4) ubiquitin ligase complexes. Deletion of *Drosophila* DCAF12 impairs larval locomotion and arrests development. At larval neuromuscular junctions (NMJs), DCAF12 is expressed presynaptically in synaptic boutons, axons, and nuclei of motor neurons. Postsynaptically, DCAF12 is expressed in muscle nuclei and facilitates Cul4-dependent ubiquitination. Genetic experiments identified several mechanistically independent functions of DCAF12 at larval NMJs. First, presynaptic DCAF12 promotes evoked neurotransmitter release. Second, postsynaptic DCAF12 negatively controls the synaptic levels of the glutamate receptor subunits GluRIIA, GluRIIC, and GluRIID. The down-regulation of synaptic GluRIIA subunits by nuclear DCAF12 requires Cul4. Third, presynaptic DCAF12 is required for the expression of synaptic homeostatic potentiation. We suggest that DCAF12 and Cul4 are critical for normal synaptic function and plasticity at larval NMJs.

Introduction

Synaptic transmission mediates rapid information transfer in neuronal circuits. The dynamic rearrangement of synaptic structure and efficacy in response to changes in neuronal activity or trophic support is critical for information processing, learning, and memory (Abbott and Regehr, 2004; Neves et al., 2008; Sjöström et al., 2008). Early studies indicate that changes in presynaptic and postsynaptic architecture and efficacy can be controlled by ubiquitination (Hegde et al., 1997; Cline, 2003), a dynamic and reversible posttranslational protein modification, which can regulate protein expression, activity, or localization. Ubiquitin-mediated signaling is regarded as a critical mechanism controlling synaptic plasticity, and its failure has been linked to numerous neurological, neurodegenerative, and psychiatric diseases (Tai and Schuman, 2008; Lehman, 2009; Mabb and Ehlers, 2010; Hegde, 2017).

The transfer of ubiquitin onto a substrate requires an enzymatic cascade including ubiquitin-activating enzymes (E1), ubiquitin-conjugating enzymes (E2), and ubiquitin ligases (E3). The most abundantly diverse components of this system are E3 ligases, which comprise hundreds of genes in mammals and are grouped into the HECT domain and RING finger families. The largest class of RING ligases are Cullin-RING finger ligases, which are assembled from a Cullin scaffold that associates with the RING finger protein to recruit an E2 enzyme and an adaptor for substrate recruitment (Petroski and Deshaies, 2005; Deshaies and Joazeiro, 2009; Lu and Pfeffer, 2014).

Vertebrates have seven Cullins. The two Cul4 paralogs (A/B) are mostly identical except for the long N terminus and nuclear localization signal (NLS) of Cul4B. Cul4 ligase complexes mediate cell cycle regulation, embryogenesis, DNA replication, DNA damage and repair, and epigenetic control of gene expression (Deshaies and Joazeiro, 2009; Hannah and Zhou, 2015). Mutations in human Cul4B have been linked to intellectual disability and epilepsy (Tarpey et al., 2007; Nakagawa and Xiong, 2011; Liu et al., 2014). Consistently, conditional Cul4B KOs show spatial learning deficits, altered dendritic properties in the hippocampus, and an increased susceptibility to stress-induced seizures (Chen et al., 2012).

Cul4A/B likely use Damaged DNA binding protein-1 (DDB1) as a unique adaptor to target substrates (Shiyanov et al., 1999b; Jackson and Xiong, 2009). Proteomic studies suggest that DDB1 links human Cul4 with >60 different potential substrate receptors termed DDB1-Cul4–associated factors (DCAFs). Of these, 52 contain a WD40 domain (Angers et al., 2006; He et al., 2006; Higa et al., 2006; Jin et al., 2006). One of these, human DCAF12, was identified as a DDB1 binding protein and component of Cul4A/B complexes (Angers et al., 2006; Jin et al., 2006; Olma et al., 2009). DCAF12 expression is altered in various human

[1]Department of Neuroscience, University of Arizona, Tucson, AZ; [2]Graduate Interdisciplinary Program in Neuroscience, University of Arizona, Tucson, AZ; [3]Department of Molecular and Cellular Biology, University of Arizona, Tucson, AZ; [4]Department of Cellular and Molecular Medicine, University of Arizona, Tucson, AZ.

Correspondence to Konrad E. Zinsmaier: kez4@email.arizona.edu.

cancer cells (Saramäki et al., 2006; Li et al., 2008), and it is required for the apoptotic elimination of supernumerary cells during *Drosophila melanogaster* metamorphosis (Hwangbo et al., 2016). However, DCAF12's role in neural and synaptic function has remained elusive.

Here, we show that presynaptic DCAF12 is required for evoked neurotransmitter release and homeostatic synaptic potentiation. Postsynaptic DCAF12 is required to down-regulate the synaptic expression of the glutamate receptor subunits GluRIIA, GluRIIC, and GluRIID. Further analysis validated a critical role of DCAF12 for Cul4-mediated protein ubiquitination and revealed that nuclear DCAF12 and Cul4 cooperate to indirectly down-regulate synaptic GluRIIA levels.

Results

Identification of lethal mutations in DCAF12

Ethyl methanesulfonate–induced recessive lethal alleles in *Drosophila* DCAF12 were identified through a genetic screen for genes that facilitate synaptic function (Guo et al., 2005). Mapping of the two alleles *B332* and *B417* identified DNA polymorphisms in the *Drosophila* orthologue of human DCAF12 (WDR40A and TCC52; Fig. 1, A–C). The *B332* allele causes an amino acid substitution (C138Y) in the first WD40 repeat, while *B417* substitutes the stop codon and adds 12 amino acids (Fig. 1 C). We also generated the CRISPR/CAS9-induced deletion $\Delta 51$ (2,008 bp), which removes the entire coding region (Fig. 1 B).

The homozygous alleles *B332* and $\Delta 51$ arrest development during late larval-to-pupal stages. In contrast, homozygous *B417* animals die during embryogenesis. Locomotion of homozygous *B332* and $\Delta 51$ third-instar larvae is significantly impaired (Fig. 1, E and F; and Fig. S2 A) and pupation is delayed by ~3–4 d. Mutant pupae lack discernible abdominal contractions and exhibit necrotic tissues (Fig. 1 D).

DCAF12 protein is expressed in neurons, glia, and muscles of *Drosophila* larvae

To determine the subcellular localization of DCAF12, we generated two polyclonal antibodies (GP11 and GP12). The GP12 specifically detects an ~55-kD protein band on Western blots of WT larval brain extracts but not *dcaf12^{\Delta 51}* deletion mutants (Fig. S1 A).

In fly larvae, DCAF12 is expressed in neurons, glia, and muscles (Figs. 2 and 3 A). In glia and neurons, DCAF12 is found in both the nucleus and cytoplasm (Fig. 2, C and O; and Fig. S1, D–I). DCAF12 expression is particularly high in axons of photoreceptors and segmental nerves exiting the ventral nerve cord (Fig. 2, A and B). In muscles, DCAF12 is primarily nuclear and prominently enriched in a few large foci (Fig. 3, A, B, D, and E). DCAF12's nuclear localization depends on its predicted NLS because overexpressed DCAF12 lacking parts of the NLS (ΔNLS; Fig. 1 C) is exclusively cytoplasmic (Fig. S1, G and H).

At larval neuromuscular junctions (NMJs), DCAF12 is essentially presynaptic (Fig. 2, D and I), where it is strongly expressed in axons and to a variable degree in synaptic boutons (Fig. 2, D–F, J, K, M, and N). Small amounts are also detectable in glial processes of NMJs (Fig. S1, I and J). In synaptic boutons, presynaptic DCAF12 does not overlap with BRP-positive active
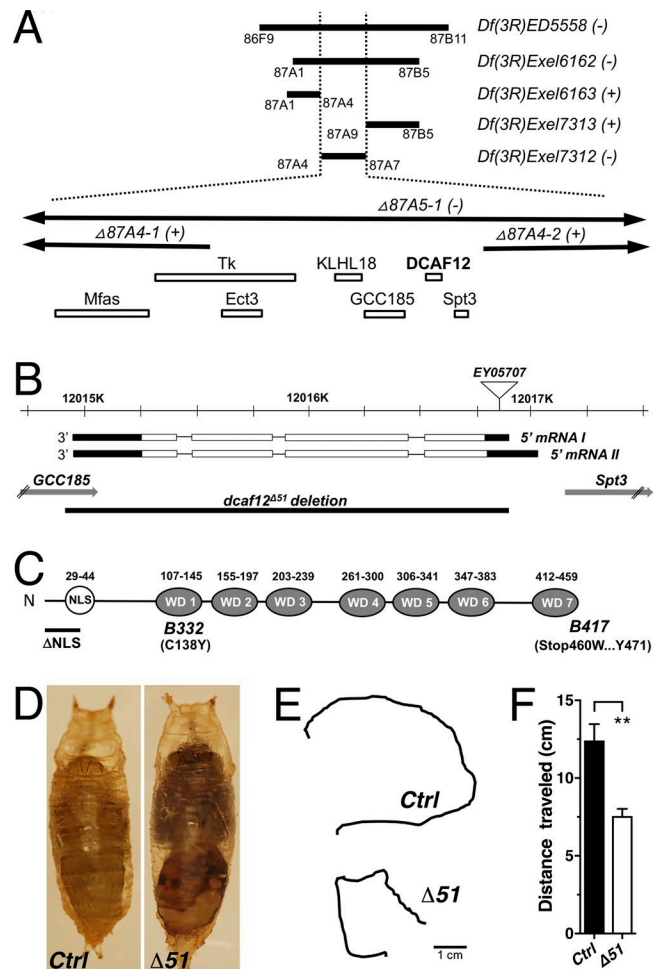

Figure 1. **Genetic and molecular analysis of DCAF12. (A)** Deficiency (Df) mapping of alleles *B332* and *B417*. Closed and open bars indicate deficiencies and genes, respectively. **(B and C)** Structure of the *dcaf12* gene and DCAF12 protein. **(D)** 3-d-old control (w^{1118}) and $\Delta 51$ mutant pupae. **(E and F)** Traces (E) and quantification (F) of crawling from control and $\Delta 51$ third-instar larvae (means ± SEM; $n \geq 6$; **, P < 0.004; two-tailed unpaired t test).

zones (AZs; Fig. 2 L). In axons, DCAF12 is associated with the plasma membrane marked by HRP and shows little overlap with Futsch-positive microtubules (Fig. 2, E–H). The residual immunofluorescence detected in axons, boutons, and nuclei of $\Delta 51$ deletion mutants is due to an unspecific cross-reactivity of the antibodies (Fig. 2, M–O).

DCAF12 forms a nuclear complex with Cul4

The focal enrichment of DCAF12 in larval muscle nuclei (Fig. 3, A and B) was reminiscent of the centrosomal localization of human DCAF12 in cancer cells (Li et al., 2008). However, in fly muscle nuclei, DCAF12-positive foci did not colocalize with the centrosomal marker γ-tubulin (Fig. 3 B); the Cajal body marker Coilin; DNA; or the nuclear proteins SMT3, Importin13, Lamin-C, Lola, and pMAD (Fig. S1 K).

Human DCAF12 has been identified as a component of Cul4 ligase complexes through its interactions with DDB1 (Angers et al., 2006; Jin et al., 2006). Consistently, GFP pull-down assays of EGFP-tagged DDB1 from *Drosophila* S2 cells extracts copurified
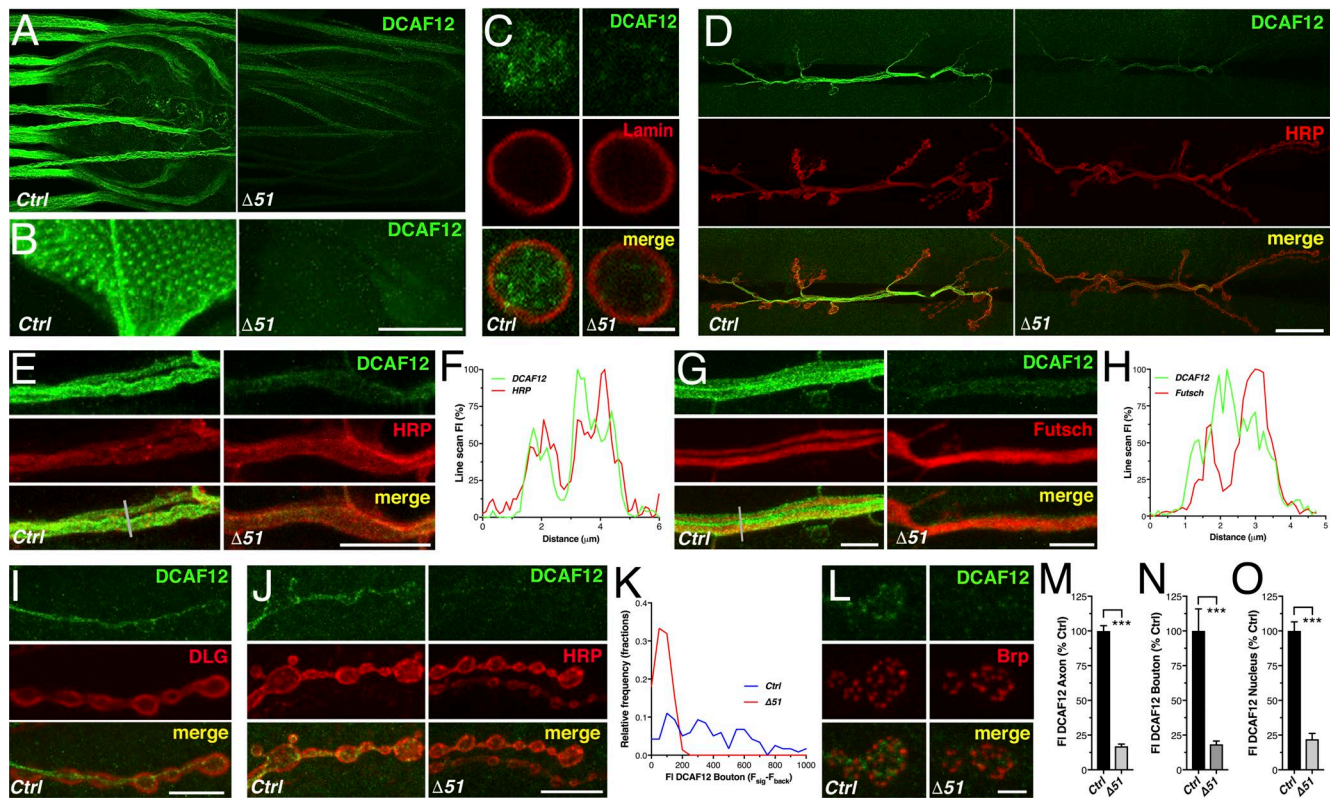
Figure 2. Subcellular localization of neuronal DCAF12. (A and B) Larval ventral nerve cord and eye disc stained for DCAF12 (GP11). **(C)** Neuronal somata stained for DCAF12 (GP12) and Lamin-C marking the nuclear envelope. **(D)** Larval NMJs stained for DCAF12 (GP11) and HRP marking the neuronal membrane. **(E and F)** Axons of NMJ (E) stained for DCAF12 and HRP and plot (F) of a single line scan (gray line in E) of DCAF12 and HRP fluorescence ($n = 1$). **(G and H)** Axons of NMJ stained for DCAF12 and Futsch (G) and plot (H) of a single line scan (gray line in G) of DCAF12 and Futsch fluorescence ($n = 1$). **(I and J)** Synaptic boutons stained for DCAF12 and postsynaptic DLG (I) or DCAF12 and HRP (J). **(K)** Frequency distribution of DCAF12 fluorescence in synaptic boutons of control ($n = 118$; $n = 3$) and $\Delta 51$ ($n = 72$; $n = 3$). **(L)** Synaptic boutons stained for DCAF12 and Brp (AZ). **(M–O)** Quantification of anti-DCAF12 fluorescence intensity (FI; means ± SEM; $n \geq 8$; ***, $P < 0.0002$; two-tailed unpaired t test). Scale bars, 50 µm (A and B), 20 µm (D), 10 µm (E, I, and J), 5 µm (C and G), and 2.5 µm (L).

V5-tagged DCAF12 (Fig. 3 I). Immunoprecipitation of flag-Cul4 from adult fly brain extracts copurified a modified ~72-kD DCAF12-positive band instead of the normal-sized 55-kD band (Fig. S1 B). Overexpression (OE) of normal and flag-tagged DCAF12 in adult fly neurons indicated that the ~72-kD band likely represents DCAF12 (Fig. S1 C).

Next, we tested whether DCAF12 colocalizes with fly Cul4. Like human Cul4B (Zou et al., 2009), fly Cul4 is mostly nuclear and enriched in a few foci that colocalized with DCAF12 (Fig. 3 B). Deletion of DCAF12 by the null allele $\Delta 51$ abolished nuclear Cul4-positive foci (Fig. 3 B). In contrast, RNAi-mediated knockdown (KD) of Cul4 abolished nuclear DCAF12 foci without affecting nuclear DCAF12 levels (Fig. 3, C, F, and G). Cooverexpressed flag-Cul4 and DCAF12 also colocalized in nuclei (Fig. 3 H). Hence, these findings suggest that DCAF12 forms distinct nuclear complexes with Cul4.

Since there are no anti-fly DDB1 antibodies available, we tested whether overexpressed myc-tagged DDB1 colocalizes with nuclear DCAF12. Consistent with the mostly cytoplasmic localization of mammalian DDB1 (Shiyanov et al., 1999a; Liu et al., 2000; Guerrero-Santoro et al., 2008; Iovine et al., 2011), the majority of myc-DDB1 was cytoplasmic in both larval neurons and muscles and did not colocalize with nuclear DCAF12 (Fig. 3 J and Fig. S1, L and M). Cooverexpression (coOE) of myc-DDB1 with DCAF12

in muscles had no effect on nuclear DCAF12's localization (Fig. S1 M). In contrast, coOE of myc-DDB1 with DCAF12 in neurons retained DCAF12 in the cytoplasm where it partially colocalized with DDB1 (Fig. S1 M). Hence, DDB1 may shuttle DCAF12 into the nucleus to facilitate its interaction with Cul4. Consistently, KD of DDB1 abolished the focal nuclear enrichment of DCAF12 and reduced nuclear DCAF12 levels (Fig. 3, C, F, and G).

DCAF12 genetically interacts with Cul4

Drosophila Cul4 is required for cell proliferation during early development (Lin et al., 2009). Consistently, Cul4 KD reduced larval muscle size (Fig. 3 N). Loss of DCAF12 had no major effects on early development. The size of larval muscles, number of nuclei, and synaptic growth of the NMJs were normal (Fig. 3, K and M; and Fig. S2, B and C); only the size of muscle nuclei was increased (Fig. 3 L). In contrast, DCAF12 OE in larval muscles impaired their structure and size, the size of nuclei, and synaptic growth of the NMJ (Fig. 3, O–R). OE of ΔNLS-DCAF12 had no significant effect (Fig. 3, P–R).

Most of the DCAF12 OE effects required Cul4 but not DDB1. Reducing Cul4 levels with a heterozygous null mutation suppressed both the muscle size and synaptic growth phenotypes but not nuclear size (Fig. 3, P–R). In contrast, reducing levels of DDB1 had no significant effect (Fig. 3, P and Q). Thus, these data indicate that both nuclear DCAF12 and Cul4 act in a common pathway.
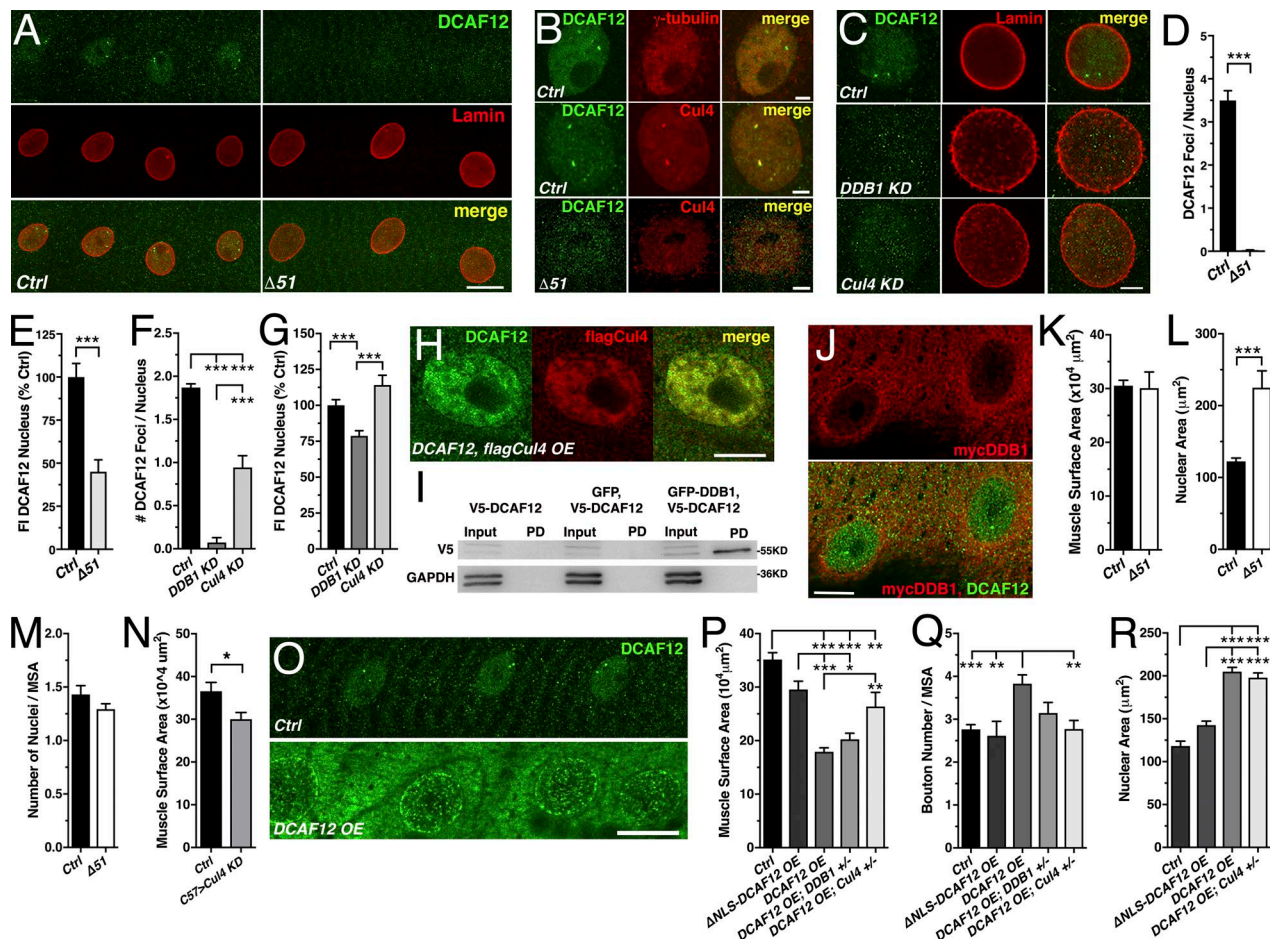
Figure 3. **Nuclear DCAF12 interacts with Cul4. (A)** Muscle nuclei stained for DCAF12 (GP11) and Lamin-C. **(B and C)** Muscle nuclei stained for DCAF12 (B and C) and γ-tubulin (B), Cul4 (B), or Lamin-C (C). **(D–G)** Amount of DCAF12 foci (D and F) and levels (E and G) in muscle nuclei ($n ≥ 35$; [D and E], $n ≥ 9$; [F and G], $n ≥ 3$). **(H)** Muscle nuclei stained for coexpressed DCAF12 and flagCul4. **(I)** Western blot of GFP pull-downs (PD) probed with anti-V5 from S2 cell extracts expressing V5-DCAF12, GFP and V5-DCAF12, or V5-DCAF12 and GFP-DDB1. GAPDH was used as a loading control. **(J)** Muscle nuclei stained for mycDDB1 and DCAF12. **(K–N)** Muscle surface area (MSA [K and N]), nuclear area (L), and normalized number (M) of nuclei ($n ≥ 11$). **(O)** Muscles stained for DCAF12. **(P–R)** Reduced Cul4 levels suppress DCAF12 OE effects on MSA (P), normalized bouton number (Q), and size (R) of nuclei ($n ≥ 6$). Scale bars, 20 µm (A and O), 10 µm (H and J), and 5 µm (B and C). Graphs display means ± SEM. Statistical analysis used two-tailed unpaired t test (E and K–N), Mann–Whitney test (D), or one-way ANOVA (F, G, and P–R); *, $P < 0.05$; **, $P < 0.01$; ***, $P < 0.001$.

DCAF12 mediates Cul4-dependent protein ubiquitination

To directly assess whether DCAF12 is either a target of Cul4-mediated ubiquitination or a cofactor of Cul4 ubiquitin ligase complexes, we examined levels of ubiquitinated proteins in *dcaf12* mutants by using antibodies that specifically detect monoubiquitinated and polyubiquitinated proteins (Fujimuro et al., 1994). Ubiquitinated protein clusters were present in the cytoplasm of control muscles, while their nuclei exhibited a much denser distribution (Fig. 4 A). Cul4 KD severely reduced the amount of ubiquitinated proteins in the nucleus (Fig. 4 A), which is consistent with the ubiquitin ligase–promoting function of fly Cul4 (Ozturk et al., 2013).
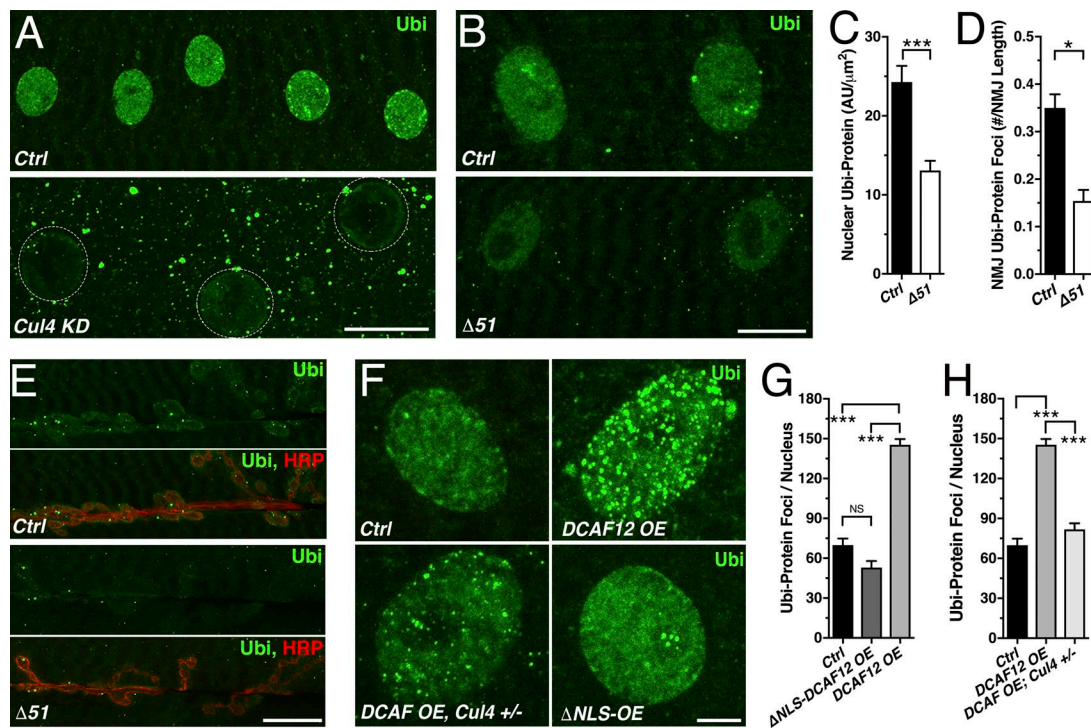
Nuclear levels of ubiquitinated proteins were reduced in *Δ51* mutants (Fig. 4, B and C), as well as levels of ubiquitinated protein foci at NMJs (Fig. 4, D and E). Conversely, DCAF12 OE increased the amount of ubiquitinated protein foci in the nucleus (Fig. 4, F–H). ΔNLS-DCAF12 OE had no significant effect relative to control (Fig. 4 G).

Reducing the gene dosage of Cul4 fully suppressed the elevated number of nuclear ubiquitinated protein foci induced by DCAF12 OE (Fig. 4, F and H) but not the increased nuclear size (Fig. 3 R). These data suggest that nuclear DCAF12 promotes Cul4-mediated ubiquitination.

Presynaptic DCAF12 is required for evoked neurotransmitter release at larval NMJs

To determine the role of DCAF12 underlying the impaired locomotion of *dcaf12* mutants (Fig. 1 F), we examined the function of larval NMJs. Loss of DCAF12 had no effect on synaptic growth, number of AZs, and levels of AZ and synaptic vesicle (SV) proteins (Fig. S2, B–F and J–L). Mutant boutons exhibited no major ultrastructural defects (Fig. S2, G–I); only the number of SVs clustered at AZs was slightly increased (Fig. S2 H).

Next, we recorded miniature excitatory postsynaptic potentials (mEPPs) and nerve-evoked EPPs. *Δ51* null mutant muscles exhibited a reduced membrane input resistance but normal

Figure 4. **DCAF12 mediates Cul4-dependent protein ubiquitination. (A and B)** Muscle nuclei (dashed circle) stained for ubiquitinated proteins (Ubi). **(C and D)** Nuclear Ubi levels in muscles (C) and number of Ubi foci (D) at NMJs ($n \geq 11$). **(E)** Larval NMJs stained for Ubi and HRP. **(F)** Muscle nuclei stained for Ubi. **(G and H)** Number of Ubi foci per nucleus ($n \geq 23$; $n \geq 7$). Scale bars, 20 µm (A and E), 10 µm (B), and 5 µm (F). Graphs display means ± SEM. Statistical analysis used two-tailed unpaired t test (C and D) or one-way ANOVA (G and H); *, $P < 0.05$; ***, $P < 0.001$.

resting potential (Fig. S3, I and J). Amplitudes of spontaneously occurring mEPPs were normal at heterozygous and homozygous $\Delta 51$ NMJs (Fig. 5, A, C, and D; and Fig. S3, A and E). The frequency of mEPPs was significantly increased in homozygous $\Delta 51$ mutants and other heterozygous and homozygous *dcaf12* alleles (Fig. 5 E and Fig. S3, D and H). However, this effect is likely due to the genetic background, as indicated by the effects of crossing in transgenes (Fig. 5 E).

Nerve-evoked EPP amplitudes at $\Delta 51$ mutant NMJs were reduced to 50–60% of control (Fig. 5, A and F). Quantal content, an estimate of the number of SVs released per given stimulus (Dodge and Rahamimoff, 1967), was also reduced (Fig. 5, G and H). However, the slope of the Ca^{2+}–quantal content relationship remained unchanged at low $_e[Ca^{2+}]$s (Fig. 5 H). Paired-pulse facilitation (EPP_2/EPP_1) was increased (Fig. 5, B and I), indicating a reduced probability of release (Regehr, 2012).

Next, we performed genetic rescue experiments using Syb- and C57-Gal4 drivers for neuron- and muscle-specific expression, respectively. Presynaptically expressed DCAF12 localized to $\Delta 51$ mutant nuclei, axons, and NMJs (Fig. S4, A and B) and hyperpolarized the muscle by ~5 mV but had no effect on membrane input resistance (Fig. S4, C and D). Postsynaptically expressed DCAF12 localized to the muscle cytoplasm and nuclei of $\Delta 51$ mutants (not shown) and had no effect on resting potential or input resistance (Fig. S4, F and G). Presynaptic, but not postsynaptic, expression of DCAF12 in $\Delta 51$ mutants restored the defects in evoked EPP amplitudes and quantal content (Fig. 5, F, G, L, and M). Taken together, these findings suggest that DCAF12 is presynaptically required for a normal probability of evoked neurotransmitter release.

Finally, we tested whether nuclear or cytoplasmic DCAF12 facilitates evoked release by expressing ΔNLS-DCAF12 in $\Delta 51$ motor neurons, which is properly localized to NMJs but absent from nuclei (Figs. S1 G and S4, A and B). Presynaptic expression of ΔNLS-DCAF12 restored evoked EPP amplitudes and partially restored quantal content at $\Delta 51$ mutant NMJs (Fig. 5, J and K). Like full-length DCAF12 (Fig. S4, C and D), ΔNLS-DCAF12 expression hyperpolarized the muscle without affecting membrane input resistance (Fig. S4, H and I). Hence, cytoplasmic and nuclear DCAF12 are required for evoked release.

Increasing neuronal excitability by reducing Mg^{2+} in the recording solution from 10 to 4 mM (Hubbard et al., 1968) partially suppressed the reduced EPP amplitudes and quantal content at homozygous $\Delta 51$ and *B332* mutant NMJs (Fig. S3, K–N). This suggests that a decreased neuronal excitability partly underlies the reduction of evoked release at *dcaf12* mutant NMJs.

Notably, we did not interpret effects of the genetically complex *dcaf12* allele *B332*. In contrast to all other alleles, heterozygous *B332* mutants exhibited dominant effects on EPP amplitudes and quantal content (Fig. S3, B and C), while homozygous *B332* mutants exhibited reduced mEPP amplitudes (Fig. S3 E) and elevated protein levels (Fig. S1 A).

Postsynaptic OE of DCAF12 impairs synaptic transmission

Presynaptic DCAF12 OE with an elav- or Ok6-Gal4 driver had no significant effects on synaptic transmission (Fig. S4, J–N). C57-driven postsynaptic OE severely impaired muscle structure (Fig. 3 O) and function (not shown), which limited recordings of mEPPs and EPPs. Reducing Gal4 activity by raising flies
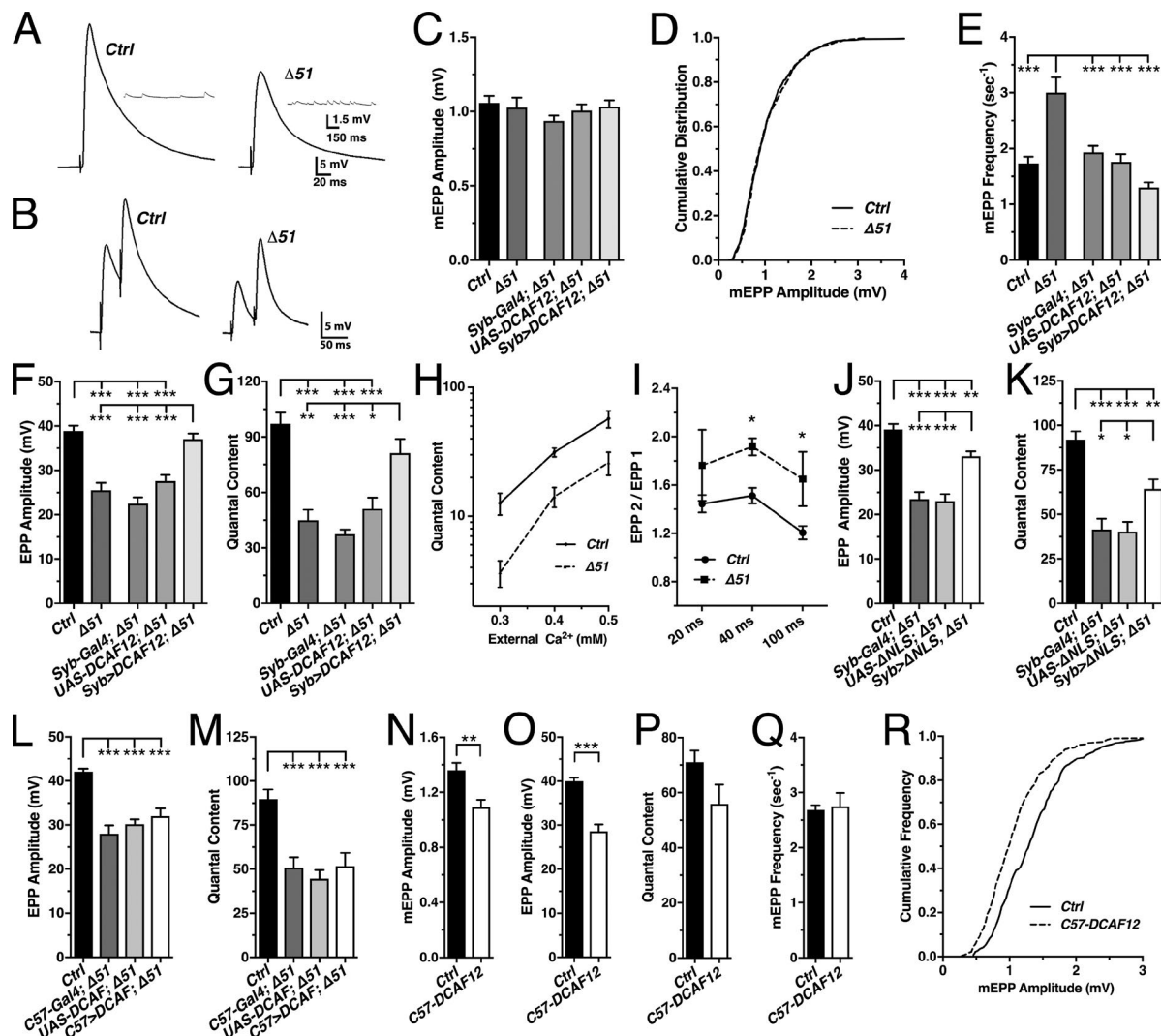
Figure 5. DCAF12 is required for evoked neurotransmitter release at larval NMJs. mEPPs and evoked EPPs were recorded from muscle 6 of the indicated genotypes in HL3 media containing 0.6 mM Ca^{2+}. **(A and B)** Representative traces of mEPPs (inset) and EPPs evoked by single- (A) or paired-pulse stimulation (B). **(C–G)** Average mEPP amplitudes (C), their cumulative frequency distribution (D; $n \geq 270$), mEPP frequency (E), EPP amplitudes (F), and quantal content (G) of control and $\Delta51$ ($n \geq 9$) and $\Delta51$ mutants expressing DCAF12 presynaptically ($n \geq 11$). **(H)** Plot of corrected quantal content recorded at various extracellular [Ca^{2+}] s ($n \geq 4$). **(I)** Paired-pulse ratio (EPP2/EPP1) for various interstimulus intervals ($n \geq 3$). **(J–M)** EPP amplitudes and quantal content from $\Delta51$ mutants expressing ΔNLS-DCAF12 presynaptically (J and K; $n \geq 9$) or DCAF12 postsynaptically (L and M; $n \geq 5$). **(N–Q)** Effects of postsynaptic DCAF12 OE on mEPP amplitudes (N), EPP amplitudes (O), quantal content (P), and mEPP frequency (Q; $n \geq 7$). **(R)** Cumulative frequency distribution of mEPP amplitudes ($n \geq 266$; $n \geq 5$). Graphs display means ± SEM. Statistical analysis used two-tailed unpaired t test (I and N–Q) or one-way ANOVA (C, E–G, and J–M); *, $P < 0.05$; **, $P < 0.01$; ***, $P < 0.001$.

at 20°C instead of 23°C to lower DCAF12 expression levels improved the electrical properties of the muscle and made stable recordings possible.

DCAF12 OE at 20°C still depolarized the muscle but had no effect on its membrane input resistance (Fig. S4, O and P). Postsynaptic DCAF12 OE reduced both mEPP and evoked EPP amplitudes (Fig. 5, N, O, and R) but had no effect on quantal content and mEPP frequency (Fig. 5, P and Q). ΔNLS-DCAF12 OE had no significant effect on mEPP amplitudes (Fig. S4 Q). Thus, nuclear DCAF12 may also have a postsynaptic role at larval NMJs.

Postsynaptic DCAF12 negatively regulates synaptic levels of GluRIIA, GluRIIC, and GluRIID subunits at larval NMJs

The effects of postsynaptic DCAF12 OE on mEPP amplitudes raised the possibility that DCAF12 controls postsynaptic GluRs.

At larval NMJs, GluRs consist of three essential subunits (GluRIIC–GluRIIE) and a variable fourth subunit, which can be either GluRIIA or GluRIIB (DiAntonio, 2006). Immunostainings revealed increased levels of GluRIIA, GluRIIC, and GluRIID at synaptic boutons of *dcaf12$^{\Delta51}$* mutants (Fig. 6, A, C, E, and F). In contrast, GluRIIB levels were normal (Fig. 6, A and D). Similar effects were present at *B332* mutant NMJs (Fig. S2, M–P). Due to a lack of antibodies, we assessed synaptic levels of transgenically expressed GFP-tagged GluRIIE, which were normal at *Δ51* mutant NMJs (Fig. 6, A and G).

Next, we examined effects on the density and size of all GluR clusters by probing for GluRIIC subunits. In comparison to control, the number of GluRIIC-positive clusters and their intensity was significantly increased at *Δ51* mutant boutons (Fig. 6, I and J). The number and density of GluR clusters containing only the
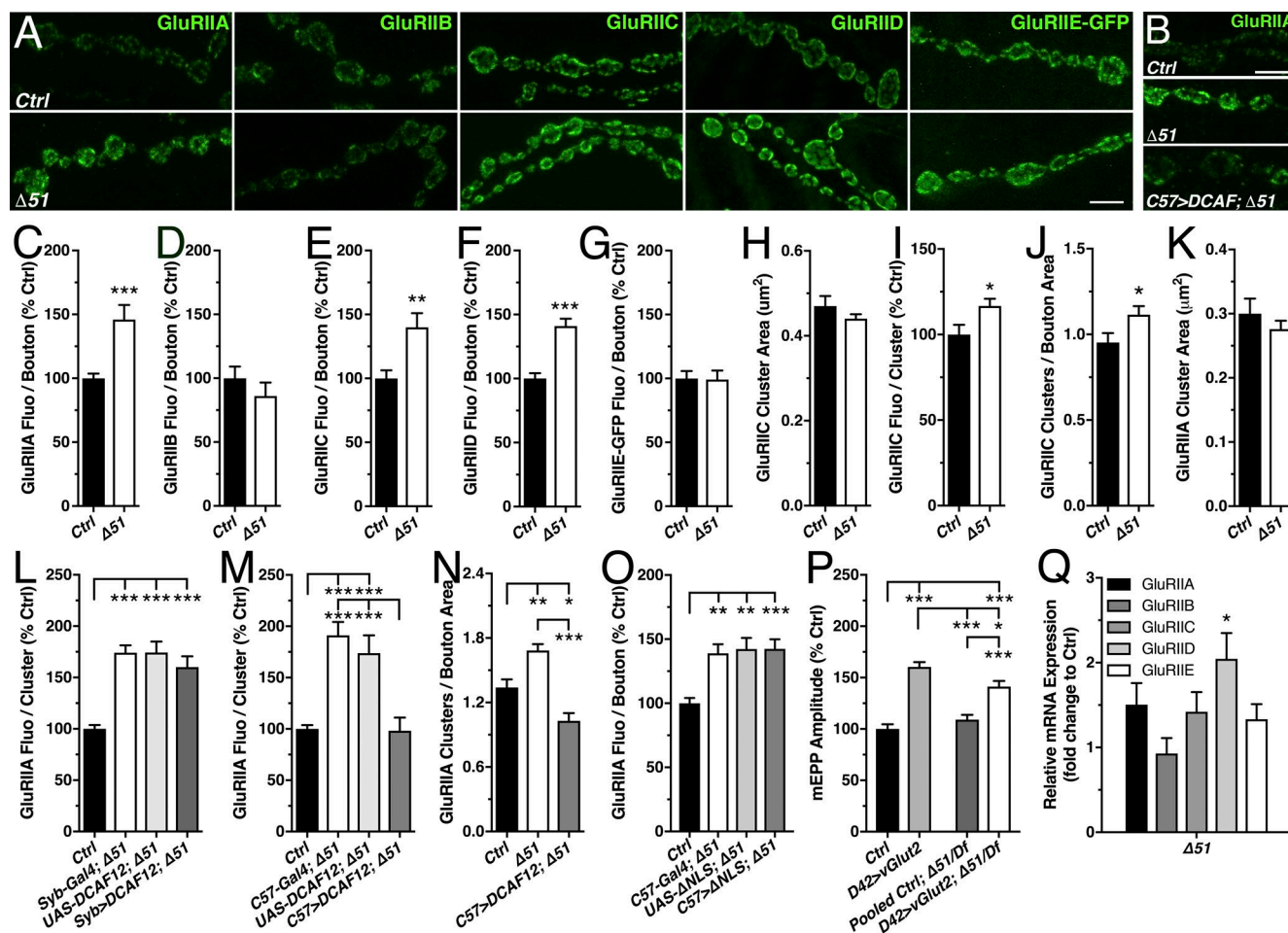
Figure 6. **Postsynaptic DCAF12 regulates the subunit composition of GluR at larval NMJs. (A and B)** Synaptic boutons of NMJs stained for endogenous GluRIIA, GluRIIB, GluRIIC, GluRIID, or overexpressed GluRIIE-GFP subunits. Scale bars, 5 μm (A) and 2.5 μm (B). **(C–G)** Effect of DCAF12 deletion on synaptic levels of endogenous GluRIIA (C; $n \geq 9$), GluRIIB (D; $n \geq 16$), GluRIIC (E; $n \geq 17$), GluRIID (F; $n \geq 13$), and overexpressed GluRIIE-GFP subunits (G; $n \geq 7$). **(H–K)** Effects of DCAF12 deletion on the size of GluRIIC-positive GluR clusters (H), GluRIIC fluorescence per cluster (I), normalized number of GluRIIC clusters to bouton area (J), and size of GluRIIA clusters (K; $n \geq 9$). **(L–O)** Effects of presynaptic (L; $n \geq 11$) and postsynaptic (M–O; $n \geq 7$) expression of DCAF12 or ΔNLS-DCAF12 in Δ51 mutants on normalized synaptic GluRIIA levels (L and M), number of GluRIIA-positive clusters per bouton area (N), and GluRIIA fluorescence per bouton (O). **(P)** Effects of vGlut OE on mEPP amplitudes ($n \geq 11$). Control is w^{1118}; pooled control includes UAS-vGlut transgene and Gal4 driver in a Δ51/Df Ex7312 background. **(Q)** GluRIIA, GluRIIB, GluRIIC, GluRIID, and GluRIIE mRNA levels in dcaf12^{Δ51} mutants normalized to control ($n \geq 5$). Graphs display means ± SEM. Statistical analysis used two-tailed unpaired t test (C–K) or one-way ANOVA (L–Q); *, $P < 0.05$; **, $P < 0.01$; ***, $P < 0.001$.

variable GluRIIA subunit was also increased (Fig. 6, M and N), but the size of both GluRIIA- and GluRIIC-positive clusters was normal (Fig. 6, H and K). This suggests that the overall increased amount of GluR clusters is likely driven by an increased number of GluRs containing GluRIIA subunits.

There are two potential explanations for the paradox that increased levels of synaptic GluRs at Δ51 mutant NMJs do not increase mEPP amplitudes. First, the increase in GluRs could be triggered by a compensatory mechanism counteracting potentially reduced SV glutamate levels. Alternatively, postsynaptic DCAF12 may facilitate the removal of dysfunctional or abnormally located GluR subunits. To distinguish between these possibilities, we tested whether presynaptic or postsynaptic DCAF12 is required for the down-regulation of GluRs.

Postsynaptic expression of DCAF12 in Δ51 mutants restored normal GluRIIA levels and reversed the elevated number of GluRIIA-containing GluR clusters to levels below control (Fig. 6, B, M,

and N) but had no effect on mEPP amplitudes (Fig. S4 E). Postsynaptic expression of ΔNLS-DCAF12 failed to restore GluR levels (Fig. 6 O), indicating that nuclear DCAF12 is required for the regulation of synaptic GluRs. Presynaptic DCAF12 expression neither restored GluR levels (Fig. 6 L) nor increased mEPP amplitudes (Fig. 5 C), as it would be expected if an increase in GluRs were to counteract reduced vesicular glutamate. These findings exclude a presynaptic mechanism and suggest that postsynaptic, nuclear DCAF12 negatively regulates synaptic levels of GluRIIA subunits.

To determine whether the abnormally accumulating GluRs of Δ51 mutant NMJs are partially dysfunctional, we tested whether increasing vesicular glutamate by presynaptic OE of the vesicular glutamate transporter (vGlut; Daniels et al., 2004) has differential effects on mEPP amplitudes at WT and Δ51 mutant NMJs. D42-driven expression increased vGlut levels at control and Δ51 mutant NMJs to a similar extent (Fig. S4 R). However, vGlut OE increased mEPP amplitudes in controls to a significantly larger
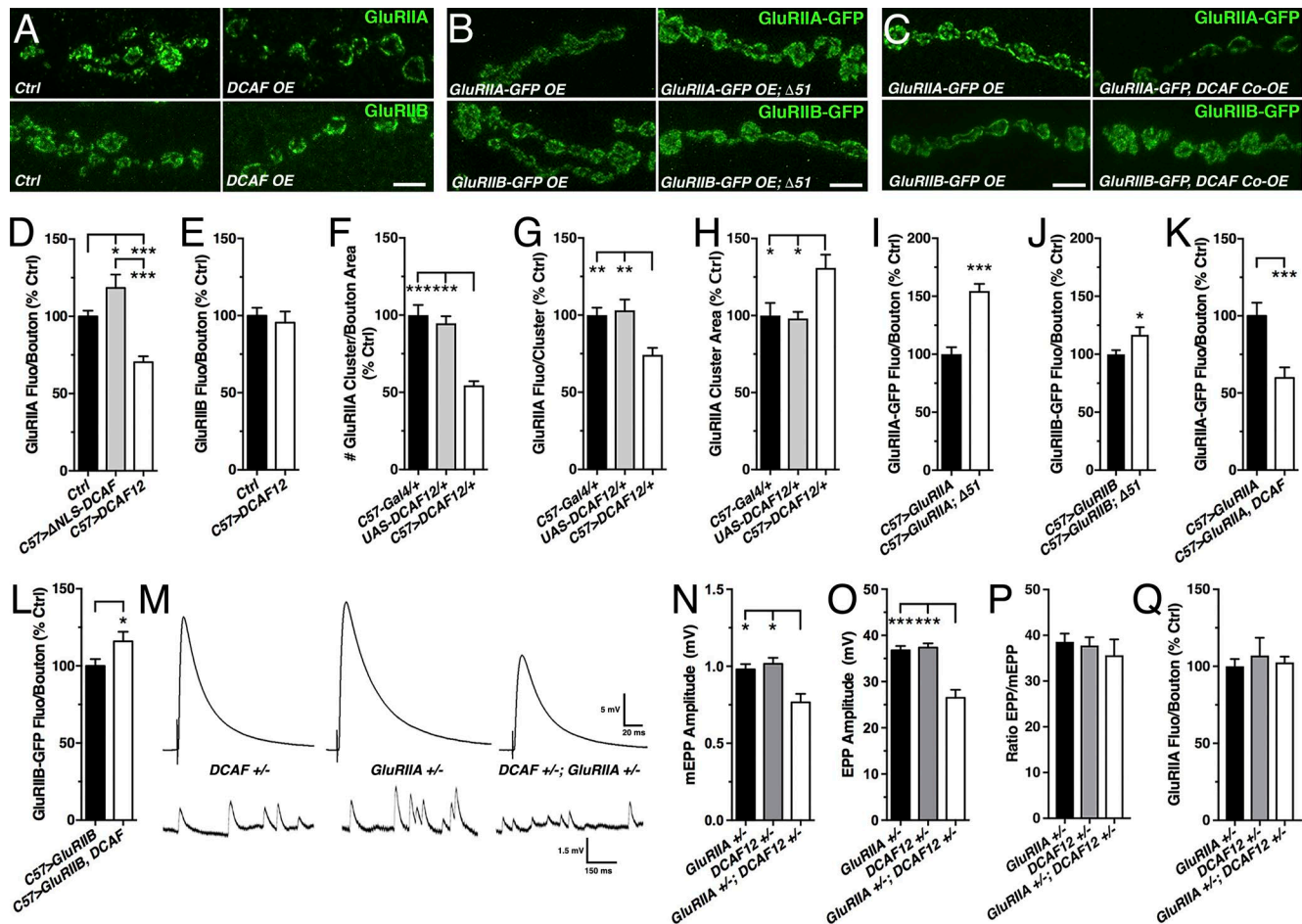
Figure 7. **Postsynaptic nuclear DCAF12 controls the synaptic ratio of GluRIIA/IIB subunits. (A–C)** Larval NMJs stained for endogenous GluRIIA and GluRIIB (A) and GFP-tagged GluRIIA and GluRIIB expressed in WT or Δ51 (B) or coexpressed with DCAF12 (C). Scale bar, 5 µm. **(D–H)** Effects of postsynaptic DCAF12 (D–H) or ΔNLS-DCAF12 OE (D) on synaptic levels of endogenous GluRIIA subunits (D and F–H; $n \geq 7$) or GluRIIB subunits (E; $n \geq 5$). **(I and J)** Effects of DCAF12 deletion on GluRIIA-GFP (I) and GluRIIB-GFP (J) expression levels ($n \geq 9$). **(K and L)** Effects of DCAF12 coOE on GluRIIA-GFP (C and K) and GluRIIB-GFP (C and L) expression levels ($n \geq 11$). **(M–Q)** Traces (M) of mEPPs and EPPs and quantification of mEPP amplitudes (N), EPP amplitudes (O), mEPP/EPP ratio (P), and synaptic GluRIIA levels (Q) from controls and trans-heterozygous glurIIA$^{SP16/+}$; dcaf12$^{Δ51/+}$ double mutants ($n \geq 7$). Graphs display means ± SEM. Statistical analysis used one-way ANOVA (D, F–H, and N–Q), two-tailed unpaired t test (I and L), or a Mann–Whitney test (E, J, and K); *, $P < 0.05$; **, $P < 0.01$; ***, $P < 0.001$.

degree than in Δ51 mutants (Fig. 6 P). This suggests that GluRs in Δ51 deletion mutants are at least partially dysfunctional, which may arise from a failure to remove dysfunctional GluRs or from a defective alignment of the accumulating GluRs with AZs.

Finally, we tested whether DCAF12 controls the expression of GluR subunits on a transcriptional level by assaying mRNA levels of all five GluR subunits using quantitative RT-PCR. Only GluRIID mRNA levels were significantly elevated in Δ51 (Fig. 6 Q) and B332 muscles (Fig. S2 Q). Thus, nuclear DCAF12 likely controls GluRIID mRNA expression.
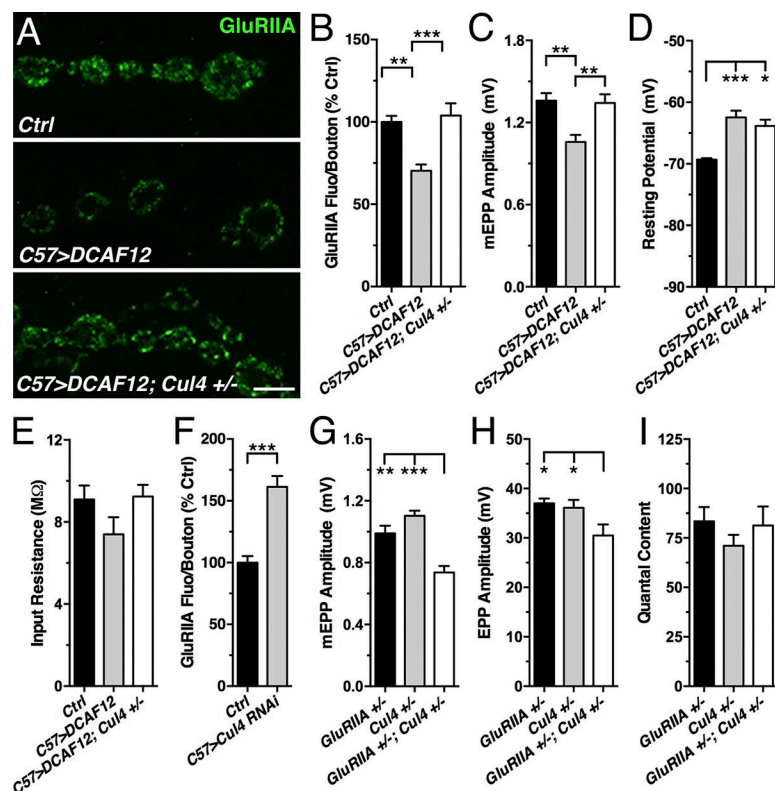
Postsynaptic DCAF12 controls the synaptic ratio of GluRIIA/B subunits by exclusively down-regulating synaptic GluRIIA
The ratio of the nonessential GluRIIA/B subunits is a critical parameter of synapse maturity at fly NMJs (Schmid et al., 2008; Jordán-Álvarez et al., 2012; Deivasigamani et al., 2015). Since loss of DCAF12 affected GluRIIA but not GluRIIB subunits (Fig. 6, C and D), we tested whether this would also be the case for DCAF12 OE. Indeed, muscle-specific DCAF12 OE reduced the

levels of GluRIIA but not GluRIIB at synaptic boutons (Fig. 7, A, D, and E). Specifically, it decreased the number and density of GluRIIA-containing GluRs, while the size of GluRIIA clusters increased (Fig. 7, F–H). The down-regulation of GluRIIA levels induced by DCAF12 OE was dependent on its nuclear localization since ΔNLS-DCAF12 OE did not reduce GluRIIA levels but instead slightly increased them (Fig. 7 D).

To confirm that DCAF12 does not regulate GluRIIA mRNA expression, we expressed GFP-tagged GluRIIA/B subunits in muscles of DCAF12 loss and gain of function mutants. Since Gal4-driven transcription is largely independent of endogenous control mechanisms, phenotypic effects on GluR-GFP expression levels are not likely to be caused by regulating mRNA expression. Postsynaptic expression levels of GluRIIA-GFP at Δ51 mutant NMJs were increased to 154% of control, while synaptic GluRIIB-GFP levels were only slightly increased (Fig. 7, B, I, and J). Similar effects were seen in B332 mutants (Fig. S2, R and S). CoOE of DCAF12 with GluRIIA-GFP or GluRIIB-GFP decreased GluRIIA-GFP levels to 60% of control, while GluRIIB-GFP levels

Figure 8. **DCAF12 controls synaptic GluRIIA levels in a Cul4-dependent manner. (A–C)** Effects of postsynaptic DCAF12 OE and reduced Cul4 on synaptic GluRIIA levels (A and B; $n \geq 11$) and mEPP amplitudes at larval NMJs (C; $n \geq 9$). Scale bar, 5 µm. **(D and E)** Effects on resting potential (D) and input resistance (E) of muscle ($n \geq 9$). **(F)** Effect of muscle Cul4 KD on synaptic GluRIIA levels ($n \geq 13$). **(G–I)** mEPP amplitudes (G), EPP amplitudes (H), and quantal content (I) of heterozygous glurIIA-cul4 double mutants ($n \geq 9$). Graphs display means ± SEM. Statistical analysis used one-way ANOVA (B–E and G–I) or two-tailed unpaired t test (F); *, $P < 0.05$; **, $P < 0.01$; ***, $P < 0.001$.

were only marginally increased (Fig. 7, C, K, and L). The latter is probably an indirect effect because the decreased GluRIIA levels may generate extra synaptic binding sites for GFP-GluRIIB due to a reduced competition with GluRIIA subunits for access to GluRIIC/D/E complexes (Marrus and DiAntonio, 2004). Taken together, these findings confirm that nuclear DCAF12 indirectly controls synaptic GluRIIA subunits through a cytoplasmic factor, consistent with the normal GluRIIA mRNA levels in *Δ51* mutants.

A role of DCAF12 for GluRIIA function was further indicated by genetic interactions. Individual heterozygous *glurIIA*[SP16/+] or *dcaf12*[Δ51/+] deletions had no effect on mEPP and EPP amplitudes (Fig. 7, M–O; and Fig. S3, A and B). GluRIIA levels in the transheterozygous double mutants were not changed (Fig. 7 Q). However, both mEPP and EPP amplitudes were proportionally decreased at transheterozygous double-mutant NMJs, since the ratio of EPP/mEPP amplitudes was not affected (Fig. 7, N–P).

DCAF12's regulation of synaptic GluRIIA levels depends on Cul4
Since nuclear DCAF12 controls synaptic GluRIIA levels, we speculated that DCAF12's role may require Cul4. Indeed, Cul4 KD in muscles increased the amount of synaptic GluRIIA subunits at larval NMJs (Fig. 8 F), indicating that Cul4 is required for the synaptic expression of GluRIIA subunits.

Cul4 was also required for the effects of postsynaptic DCAF12 OE on synaptic GluRIIA levels and mEPP amplitudes. Reducing the gene dosage of Cul4 by one copy restored both synaptic GluRIIA levels and mEPP amplitudes to control levels (Fig. 8, A–C) but had no significant effect on the resting potential and membrane input resistance relative to DCAF12 OE (Fig. 8, D and E).

A critical role of Cul4 was further supported by genetic interactions. mEPP and EPP amplitudes were normal at both heterozy-

gous *glurIIA*[SP16/+] and *cul4*[11L/+] NMJs but significantly decreased at transheterozygous double-mutant *glurIIa*[SP16/+]; *cul4*[11L/+] NMJs (Fig. 8, G and H). Quantal content remained normal (Fig. 8 I). These data indicate that nuclear DCAF12 controls postsynaptic GluRIIA levels by a Cul4-dependent mechanism.

DCAF12 is required for homeostatic potentiation of evoked release at larval NMJs
Next, we explored whether DCAF12 mediates homeostatic potentiation of synaptic transmission. This form of synaptic plasticity maintains normal postsynaptic excitation in response to a decrease in postsynaptic neurotransmitter receptor sensitivity and requires transsynaptic signaling to up-regulate evoked release (Petersen et al., 1997; DiAntonio et al., 1999; Davis, 2006; Turrigiano, 2012; Frank, 2014). At fly NMJs, loss of both GluRIIA and GluRIIC subunits triggers a homeostatic increase in quantal content to maintain evoked EPP amplitudes (Petersen et al., 1997; DiAntonio et al., 1999; Marrus and DiAntonio, 2004; Brusich et al., 2015).

To test whether homeostatic signaling requires DCAF12, we generated homozygous *GluRIIA-DCAF12* double-mutant flies, which unexpectedly died at much earlier developmental stages than each individual mutant. Only a very small number survived to the early third-instar stage. These exhibited reduced EPP amplitudes and quantal content (Fig. S5, A–D), as seen in individual *dcaf12* mutants. Accordingly, loss of GluRIIA subunits in the double mutants did not trigger a homeostatic response. However, this could have been a consequence of the primary evoked release defect of *dcaf12* mutants.

To bypass the confounding problem of impaired basal transmission, we tested whether reducing the gene dosage of DCAF12
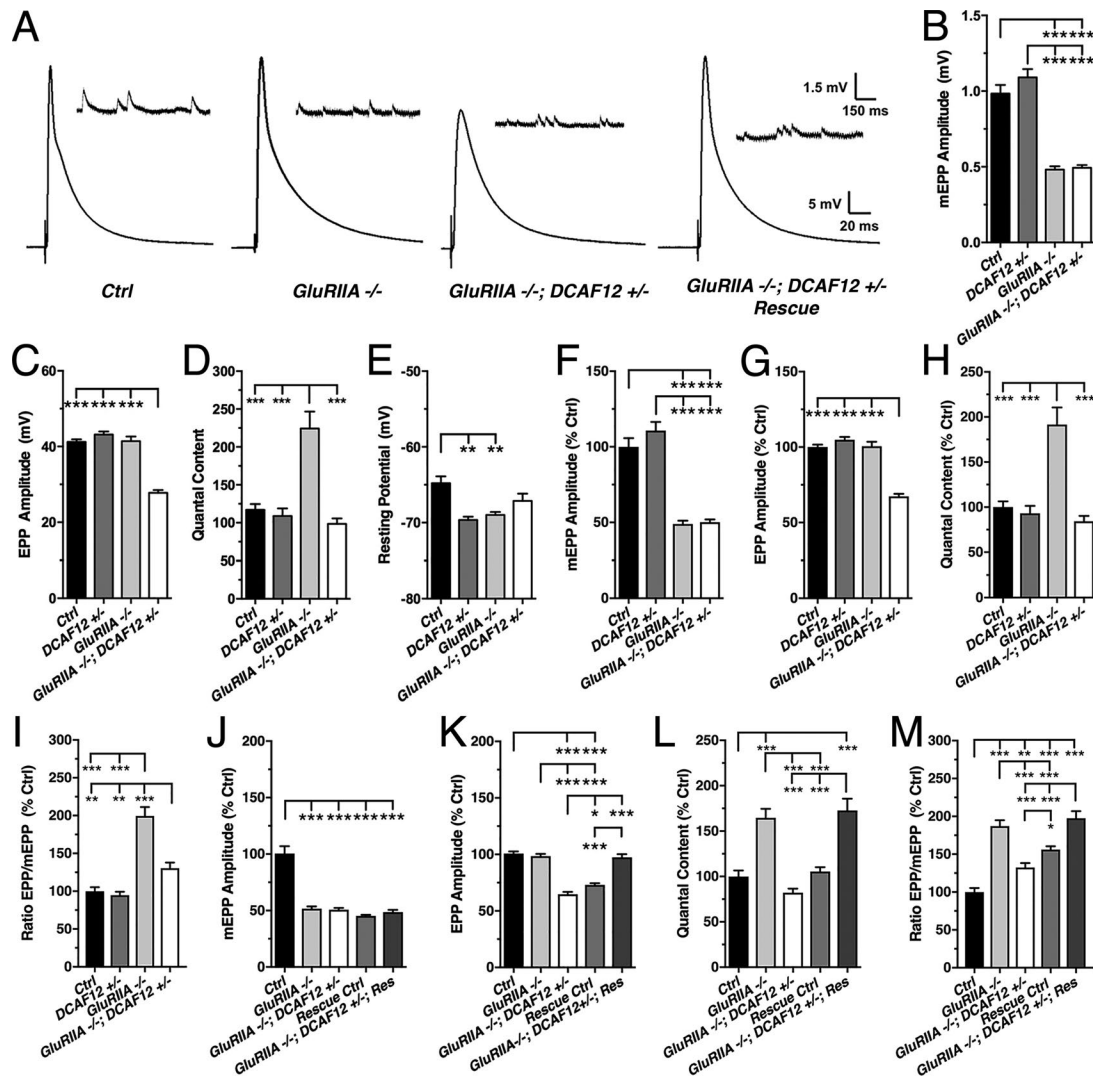
Figure 9. **Presynaptic DCAF12 is required homeostatic potentiation.** mEPPs and EPPs were recorded from larval muscle 6 of indicated genotypes in HL3 media containing 0.6 mM Ca²⁺. **(A)** Representative traces of mEPPs (inset) and EPPs. **(B–I)** Effects of reducing DCAF12 in *glurIIA^SP16* mutants on average and normalized mEPP amplitudes (B and F), EPP amplitudes (C and G), quantal content (D and H), EPP/mEPP ratio (I), and muscle resting potential (E; $n \geq 8$). **(J–M)** Effects of genetic rescue of DCAF12 on normalized mEPP amplitudes (J), EPP amplitudes (K), quantal content (L), and EPP/mEPP ratio (M; $n \geq 14$). Graphs display means ± SEM. Statistical analysis used one-way ANOVA (B–M); *, $P < 0.05$; **, $P < 0.01$; ***, $P < 0.001$.

suppresses the compensatory increase in quantal content of homozygous *glurIIA^SP16* mutants (Fig. 9, D and H). In comparison to individual *glurIIA^SP16* mutants, removing one gene copy of DCAF12 had no effect on mEPP amplitudes and the resting membrane potential (Fig. 9, A, B, E, and F). However, it significantly reduced evoked EPP amplitudes due to a partial suppression of the homeostatic increase in the ratio of mEPP/EPP amplitudes and quantal content (Fig. 9, A, C, D, and G–I).

Next, we performed genetic rescue experiments. Rescue controls containing either a silent UAS-DCAF12 transgene or the Syb-Gal4 driver had no effect on mEPPs, EPPs, and quantal content (Fig. 9, J–M). Presynaptic expression of DCAF12 in *glurIIA^SP16*; *dcaf12^Δ51/+* double mutants had no effect on mEPP amplitudes (Fig. 9, A, and J; and Fig. S5 E). However, it restored evoked EPP amplitudes to levels that were similar to control and *glurIIA^SP16* mutants (Fig. 9, A and K, and Fig. S5 F). The effect on EPPs was due to a rescue of the homeostatic increase in quantal content,

which was similar to that of *glurIIA^SP16* mutants (Fig. 9, L and M; and Fig. S5 G). Presynaptic DCAF12 expression caused a slight hyperpolarization of the muscle similar to that of individual *glurIIA^SP16* mutants (Fig. S5 H). Postsynaptic rescue experiments were deemed not informative due to the confounding effect of postsynaptic DCAF12 OE on GluRs. These data suggest that presynaptic DCAF12 is required for the expression of homeostatic potentiation at larval NMJs.

Discussion

Our study identified novel synaptic roles of DCAF12, a potential cofactor of Cul4 E3 ligase (Angers et al., 2006; Jin et al., 2006; Olma et al., 2009). Loss of DCAF12 arrests development and impairs larval locomotion. Presynaptic DCAF12 facilitates neurotransmitter release and synaptic homeostasis, while postsynaptic nuclear DCAF12 is required to maintain synaptic GluRIIA,

GluRIIC, and GluRIID levels. In addition, we demonstrate a critical role of nuclear DCAF12 for Cul4-mediated protein ubiquitination and show that DCAF12 together with Cul4 negatively controls synaptic GluRIIA levels.

Nuclear DCAF12 associates with Cul4 promoting protein ubiquitination

Affinity purifications using Cul4A, DDB1, or chromatin-associated DDA1 indicated that DCAF12 can associate with Cul4A/B complexes together with components of the COP9 signalosome (Angers et al., 2006; Olma et al., 2009), which likely inactivates various Cullin ligases by deneddylation (Wee et al., 2005; Wu et al., 2005). However, the role of Cul4-associated DCAF12 has remained speculative. DCAF12 could link ubiquitination substrates to Cul4 (Angers et al., 2006; He et al., 2006; Higa and Zhang, 2007), could modulate the E3 ubiquitin ligase activity, or could be a ubiquitination target of Cul4.

We confirmed the biochemical interaction of DCAF12 with DDB1 in S2 cells and with Cul4 in adult fly brains. In addition, immunostainings suggest that DCAF12 forms a nuclear protein complex with Cul4 in muscles, where they are enriched in distinct foci. This focal enrichment requires normal levels of Cul4, DDB1, and DCAF12. The nature of the DDB1 interaction with DCAF12 and Cul4 remains to be further explored, but it is possible that DDB1 may stabilize DCAF12-Cul4 complexes and/or aid shuttling of DCAF12 into muscle nuclei.

Further genetic studies showed that loss of DCAF12 and Cul4 reduced ubiquitinated nuclear protein levels. Vice versa, DCAF12 OE increased nuclear protein ubiquitination. This DCAF12 OE effect was suppressed by reducing the gene dosage of Cul4, indicating that DCAF12 promotes Cul4 protein ubiquitination. The possibility that DCAF12 is ubiquitinated by Cul4 complexes for degradation can be excluded since Cul4 KD had no effect on DCAF12 levels.

DCAF12 is required for pre- and postsynaptic function at larval NMJs

We suggest that neuronal DCAF12 is cell-autonomously required for evoked neurotransmitter release because DCAF12 expression in *dcaf12* mutant motor neurons fully restored the loss of evoked release at NMJs. DCAF12 likely promotes a Ca^{2+}-dependent step of release since its loss reduced the Ca^{2+} sensitivity of release and increased paired-pulse facilitation. Because cytoplasmically localized ΔNLS-DCAF12 partially restored evoked release in *dcaf12* mutants, we suggest that DCAF12 is required for both nuclear and cytoplasmic mechanisms in neurons. Next to controlling mechanisms of evoked release, DCAF12 may also facilitate neuronal excitability by regulating ion channels since lowering $[Mg^{2+}]$ improved evoked release in *dcaf12* mutants. Consistently, Cul4 ubiquitinates large-conductance Ca^{2+}-activated potassium (BK) and CLC-1 chloride channels (Chen et al., 2015; Song et al., 2018).

Postsynaptically, DCAF12 is required for a normal composition of synaptic GluRs by negatively controlling the levels of GluRIIA, GluRIIC, and GluRIID, which accumulated in *dcaf12* mutants. Paradoxically, the increased levels of synaptic GluRs at *dcaf12* null mutant NMJs did not increase mEPP amplitudes. This raised the possibility that the accumulating GluRs are either dysfunctional or the product of a compensating response to a presynaptic defect in the glutamate content of SVs. However, the latter was not the case since presynaptic expression of DCAF12 in *dcaf12* mutants did not affect GluR levels or increased mEPP amplitudes. Only postsynaptic expression restored normal synaptic GluR levels, as exemplified by GluRIIA subunits. Hence, the abnormally accumulating GluRs are likely dysfunctional or mislocalized. This possibility was supported by the differential effects of presynaptic vGlut OE, which increased mEPP amplitudes in controls to a significantly larger degree than in *Δ51* mutants.

Finally, RT-PCR assays showed that only GluRIID mRNA levels are significantly elevated in *dcaf12* muscles, indicating that DCAF12 controls synaptic GluRIID expression on a transcriptional level. In contrast, nuclear DCAF12 may control at least synaptic GluRIIA levels through the transcriptional control of an unknown postsynaptic factor that regulates synaptic GluRIIA levels. This idea is supported by the effects of altered DCAF12 levels on the Gal4-driven expression of GluRIIA-GFP.

DCAF12 controls the ratio of GluRIIA/B subunits in a Cul4-dependent manner

Loss and OE of DCAF12 exclusively affected GluRIIA but not GluRIIB. This differential effect is particularly interesting because these subunits determine the Ca^{2+} permeability and kinetic properties of GluRs (DiAntonio et al., 1999; Schmid et al., 2008; Han et al., 2015). Moreover, the ratio of GluRs containing either GluRIIA or GluRIIB subunits determines the developmental maturity of postsynaptic densities of larval NMJs and is critical for activity-dependent synaptic plasticity (Petersen et al., 1997; DiAntonio et al., 1999; Schmid et al., 2008).

The elevated synaptic levels of GluRIIA subunits at both *dcaf12* mutant NMJs could have been due to a presynaptic defect since the developmental switch toward a more balanced GluRIIA/B ratio is induced by the maturation of the presynaptic AZ and subsequent association of additional Ca^{2+} channels (Schmid et al., 2008; Sulkowski et al., 2014). However, this is unlikely to be the case for three reasons: First, *dcaf12* mutant NMJs exhibited a normal number of AZs and BRP levels. Second, GluRIIA levels of *dcaf12* null mutants were restored by postsynaptic but not presynaptic expression of normal DCAF12. Third, postsynaptic DCAF12 OE decreased synaptic GluRIIA levels. Hence, postsynaptic DCAF12 is likely a negative regulator of synaptic GluRIIA levels. Genetic interactions between heterozygous deletions of *glurIIA* and *dcaf12* further support this notion.

Consistent with DCAF12's nuclear localization, genetic rescue and OE experiments using ΔNLS-DCAF12 confirmed that nuclear DCAF12 controls synaptic GluRIIA levels. Since *dcaf12* mutants had no effect on GluRIIA mRNA levels, nuclear DCAF12 controls synaptic GluRIIA levels indirectly through a third factor. This was substantiated by the effects of loss and OE of DCAF12 synaptic GFP-GluRIIA levels, which were altered like endogenous GluRIIA levels.

Mechanistically, DCAF12's inhibitory control of GluRIIA expression depends on Cul4, which is indicated by three critical observations: (1) Cul4 KD in muscles increased synaptic GluRIIA levels at the NMJ. (2) Heterozygous *cul4-glurIIA* double mutants exhibited reduced mEPP amplitudes, indicating that Cul4 and

GluRIIA act in a common pathway. (3) Reducing the gene dosage of Cul4 fully suppressed the increased levels of synaptic GluRIIA subunits induced by DCAF12 OE. Taken together, we suggest that a nuclear DCAF12-Cul4 E3 ubiquitin ligase complex controls a transcription factor for the expression of an unknown cytoplasmic factor down-regulating synaptic GluRIIA levels. An intriguing synaptic candidate whose mRNA expression may be controlled by DCAF12-Cul4 is the multimeric Cul3-Kel8 ubiquitin ligase complex, which ubiquitinates the synaptic GluR subunit GLR-1 for degradation in *Caenorhabditis elegans* (Schaefer and Rongo, 2006).

DCAF12 is required for synaptic homeostasis at larval NMJs

Homeostatic synaptic plasticity is critical for maintaining stable neuronal networks (Turrigiano, 2012; Davis and Müller, 2015). Several pieces of genetic evidence suggest that presynaptic DCAF12 is critically required for synaptic homeostasis at larval NMJs. (1) Analysis of homozygous *glurIIA-dcaf12* double mutants revealed no homeostatic response as it is typically observed in individual *glurIIA* mutants. (2) Reducing the gene dosage of DCAF12 impaired the compensatory homeostatic increase in quantal content of homozygous *glurIIA* mutants. (3) Presynaptic expression of DCAF12 restored quantal content, indicating that presynaptic DCAF12 is required for maintaining synaptic homeostasis. Notably, DCAF12 is required at the larval NMJ for two independent mechanisms of synaptic plasticity. Since proteasomal function is required for homeostatic potentiation (Wentzel et al., 2018), it is conceivable that DCAF12 may regulate presynaptic homeostasis via a ubiquitin- and Cul4-dependent mechanism.

In conclusion, this study extends the repertoire of proteins facilitating synaptic function and plasticity. It also illuminates the importance of expanding our understanding of Cul4-mediated ubiquitination for GluR function and plasticity. A further understanding of DCAF12's pleiotropic synaptic functions may shed light on how potentially cross-linked molecular pathways work together to orchestrate stable cellular networks and how alterations in these pathways can lead to Cul4B-mediated intellectual disability in humans (Tarpey et al., 2007; Zou et al., 2007).

Materials and methods

Drosophila stocks and husbandry

All flies were raised at 23°C on standard cornmeal medium with a 12/12-h light–dark cycle unless otherwise specified. Strains P{XP}CG18547[d05047], P{WH}Tk[f06233], P{XP}CG18547[d05047], PBac{WH}f00760, and P{XP}d08712 were obtained from Bloomington *Drosophila* Stock Center (BDSC) and the Exelixis collection at Harvard Medical School. UAS hairpin strains to KD DCAF12 (43758), DDB1/piccolo (44974 and 44976), and Cul4 (105668KK) were obtained from the Vienna *Drosophila* RNAi Center. The *cul4[11L]* and *ddb1[EY01408]* strains were obtained from Robert Duronio (University of North Carolina, Chapel Hill, NC). The Gal4 driver strains C57/BG57-Gal4 and nSyb-Gal4 were obtained from Vivian Budnik (University of Massachusetts, Amherst, MA) and Hugo Bellen (Baylor College of Medicine, Houston, TX), respectively. GFP-tagged UAS

transgenes expressing GFP-GluRIIA, GFP-GluRIIB, and GFP-GluRIIE were obtained from Stephan Sigrist (Freie Universität Berlin, Berlin, Germany). UAS-vGlut2 was obtained from Aaron DiAntonio (Washington University, St Louis, MO). The *glurIIA[SP16]* strain was obtained from C. Andrew Frank (University of Iowa, Iowa City, IA).

Deficiency mapping

Standard deficiency mapping using the BDSC deficiency kit for chromosome 3R was used to map the genetic locus of the lethal alleles *B332* and *B417* to the deletion *Df(3R)Exel7312* by testing the viability of the respective heteroallelic combinations. The small deletion alleles *Δ87A4-1*, *Δ87A4-2*, and *Δ87A5-1* were used to further narrow down the mapping interval. These alleles were generated by FRT-mediated recombination (Parks et al., 2004). Specifically, *Δ87A4-1* was generated by crossing the FRT insertion P{XP}CG18547[d05047] to a heat shock–driven FLP recombinase (hs-FLP; *P{hsFLP}1, y[1] w[1118]; Dr[Mio]/TM3*) at 25°C. F1 progeny (*P{hsFLP}1, y[1] w[1118]; P{XP}CG18547/TM3*) containing hs-FLP and the FRT insertion were crossed to P{WH}Tk[f06233] to generate F2 progeny containing two FRT insertions in trans in the presence of hs-FLP (*P{hsFLP}1, y[1] w[1118]; P{XP}CG18547/P{WH}Tk*). After 2 d, crosses (parents and progeny) were subjected to a 1-h heat shock by placing the bottles into a 37°C water bath. Parents were removed after 1 d, and bottles were subjected to four more daily 1-h heat shocks. Progeny were raised to adulthood, and individual virgin females were crossed to marked balancer chromosomes. Individual male progeny were then crossed to females to generate additional progeny for PCR confirmation analysis and to balance the stocks. The deletions *Δ87A4-2 and Δ87A5-1* were generated accordingly using the FRT insertions P{XP}CG18547[d05047] and P{WH}f00989, and PBac{WH}f00760 P{XP}d08712, respectively.

DCAF12 antibody generation

Drosophila DCAF12 cDNA was PCR amplified from clone LD21841 (*Drosophila* Genomics Resource Center [DGRC]) using forward (5′-GAGA*GCTAGC*TTCAACGGGATGGTGAGAACCATCCGCG-3′) and reverse primers (5′-GA*GAATTC*CTATTGCCAAACGCCCGCATAGTTGCC-3′) containing *Nhe*I and *Eco*RI restriction sites (sites are underlined in primer sequences), respectively. DCAF12 cDNA was then subcloned in frame to the N-terminal 6xHis-tag of the vector pET28b (Novagen) using *Nhe*I and *Eco*RI restriction enzymes. The recombinant fusion protein was expressed in *Escherichia coli* BL21 (DE3) cells (Invitrogen) and purified from cell lysates using the PrepEase His-tagged protein purification kit (Affymetrix/USB). Two guinea pigs (GP11 and GP12) were immunized for polyclonal antibody production using a 90-d protocol (Cocalico Biologicals). The obtained antisera were screened by immunohistochemistry and Western blotting using larval protein extracts.

Generation of UAS transgenes

To generate a transgene encoding full-length DCAF12, cDNA was PCR amplified from clone LD21841 (DGRC) with primers containing either an *Eco*RI and Kozak sequence (5′-GG*AATTC*GCCACCATGTTCAACGGGATGGTGAGAACCATCCGCGACAGCG-3′) or a *Xho*I site (5′-GC*CTCGAG*CTATTGCCAAACGCCCGCATAGTTGCC

Patrón et al.
DCAF12's pleiotropic synaptic functions

Journal of Cell Biology 1004
https://doi.org/10.1083/jcb.201805099

CACCAAAGTCGC-3') and subcloned into a pUAST vector (Brand and Perrimon, 1993), using EcoRI and XhoI sites.

To generate a transgene expressing ΔNLS-DCAF12, cDNA was PCR amplified from clone LD21841 using forward and reverse primers containing either a flanking NotI and Kozak sequence (5'-GAGAGCGGCCGCGACAAAATGCGACAGGAGCGTAGACGA AAACCGG-3') or a XbaI site (5'-GAGA TCTAGACTATTGCCAAAC GCCCGCATAGTTGCCC-3'), and subcloned into a pUAST vector using NotI and XbaI sites. The resulting cDNA transgenes encode an N-terminally truncated DCAF12 protein, which lacks the first 35 amino acids, including 7 amino acids (underlined) of the NLS (RRAKQRAMRQERRRK) and starts at position M36.

To generate a transgene encoding N-terminal FLAG-tagged Cul4, cDNA was PCR amplified from clone LP02965 (DGRC) using forward and reverse primers containing a flanking NotI (5'-GA GAGCGGCCGCAGTGCGGCCAAGAAGTACAAGCCCATGG-3') or KpnI site (5'-GAGAGGTACCTTATGCCACATAGTTGTATTGGTT TTGATTATCCTTGTCTCGCTCC-3') and subcloned into a FLAG-tagged pUAST vector using NotI and KpnI sites. pUAST-FLAG was generated by annealing two complementary oligomers encoding the FLAG epitope (5'-AATTCACCGGTGACAAAATGGATTATAAAG ATGATGATGATAAAGC-3'; 5'-GGCCGCTTTTATCATCATCATCTT TATAATCCATTTTGTCACCGGTG-3'), cutting them with EcoRI and NotI and cloning them into an equally cut pUAST vector.

To generate a transgene encoding N-terminal myc-tagged DDB1/piccolo, a 6x-myc tag-containing pUAST vector was generated PCR-amplifying a 6x-myc tag sequence from a pTMW vector (DGRC) using primers containing EcoRI (5'-TAGAATTCGAC AAAAGGCCTGTCTAGAGAAGCTCCGCCACC-3') or BglII sites (5'-TAAGATCTCGTTTCTCGTTCAGCTTTTTTGTACAAACTTGTATA CCGGTG-3'). The amplified 6x-Myc tag DNA was cut with EcoRI and BglII and subcloned into a pUAST vector. DDB1 cDNA was PCR amplified from clone LD08715 (DGRC) using primers containing flanking NotI (5'-TAGCGGCCGCTTCGCATCACTACGTGGT GACGGCGC-3') or KpnI sites (5'-TAGGTACCTCAATGCATGCGCGT GAGGTCCTCGAC-3'). The amplified DDB1 cDNA was cut with NotI and KpnI and inserted in frame to the 6x-myc tag sequence of the modified pUAST vector.

pUAST-x plasmids were injected into w[1118] embryos (Rainbow Transgenic Flies). At least two independent recombinant strains were obtained for each transgene. Recombinant flies were outcrossed to w[1118] to exchange nonrecombinant chromosomes. Homozygous strains containing UAS-transgenes were established in a WT control (w[1118]) and/or dcaf12 mutant genetic background.

Generation of a CRISPR-mediated DCAF12 deletion allele
A deletion allele of DCAF12 (Δ51) was generated by using the CRISPR/CAS9 System. CRISPR target sites for DCAF12 were identified using the CRISPR Optimal Target Finder Tool (Gratz et al., 2014). Two chiRNAs targeting the 5' and 3' ends of DCAF12 were used to generate a large deletion of the dcaf12 gene. Plasmids encoding chiRNAs 1 (oligo 1–2) and 2 (oligo 3–4) were generated by using the U6-gRNA CRISPR protocol (Gratz et al., 2013) and the following PCR primers: oligo 1, 5'-CTTCGTAGACTACAGTGGAAC TAC-3'; oligo 2, 5'-AAACGTAGTTCCACTGTAGTCTAC-3'; oligo 3, 5'-CTTCGATTTATAGTCTGATCTATA-3'; and oligo 4, 5'-AAACTA TAGATCAGACTATAAATC-3'. The chiRNA plasmids were in-

jected into CAS9 expressing embryos (y[1] M{vas-Cas9}ZH-2A w[1118]/FM7c; BDSC no. 51323) to generate DCAF12 deletion animals (Rainbow Transgenic Flies). The extent of the deletion was confirmed by PCR analysis and sequencing using the forward primers GFwd1 (5'-GAAAGCGATGGCCTATCGTTAGGGATG AACG-3') and PFwd1 (5'-CGCACCACCATTTTTGTTTGCGGATGA TAACCCG-3'), and the reverse primer R1 (5'-CCACACCCGTTG TGTTGAGTGCCCT-3').

Quantitative RT-PCR
RNA was isolated from muscle extracts of third-instar larvae reared at 23°C using the Quick-RNA Microprep Kit with on-column DNase treatment (Zymo Research). cDNA synthesis was performed with a SuperScript VILO cDNA Synthesis Kit (no. 11754050; Thermo Fisher Scientific). Quantitative PCR was conducted with a Power SYBR Green PCR Master Mix (no. 4368577; Thermo Fisher Scientific) using a StepOnePlus Real Time PCR System (Applied Biosystems). Melt curve analysis verified the presence of a single product for all reactions. Mean cycle threshold (CT) of triplicate reactions was used to determine relative expression of target genes using 2-ΔCT method (Pfaffl, 2001). The following primer pairs were used: GluRIIA, forward: 5'-CCA CTGGGCTCTGATTACCG-3'; reverse: 5'-CCAGAACAAGAAACA CGCCG-3'; GluRIIB, forward: 5'-GGAGAAGATTCCACCCATGCT-3'; reverse: 5'-TTGAATCCCGACTTTGGCGA-3'; GluRIIC, forward: 5'-GGACTGGGAGAACCCACATC-3'; reverse: 5'-CATTCGCACCTG TGGACTTC-3'; GluRIID, forward: 5'-TACTCGAATACCAGAGGA CGGA; reverse: 5'-GATGAGGCCCAGGCGAATG-3'; GluRIIE, forward: 5'-TGGAGCCTTTTTAGCATTCACA-3'; reverse: 5'-GTCGGT GAGCAGACCTATGG-3'; and RP49, forward: 5'-ATGCTAAGCTGT CGCACAAATG-3'; reverse: 5'-GTTCGATCCGTAACCGATGT-3'.

Immunostainings and confocal imaging
Wandering third-instar larvae were dissected in Sylgard-coated dishes containing HL3 solution (70 mM NaCl, 5 mM KCl, 10 mM MgCl$_2$, 10 mM NaHCO$_3$, 5 mM Trehalose, 115 mM sucrose, and 5 mM Hepes, pH 7.3) and fixed for 20 min in 4% formaldehyde (Electron Microscopy Sciences) in PBS (pH 7.3) at RT. GluRIIA and vGlut stainings required fixation for 3–5 min with Bouin's Fix (Ricca Chemical Company). After washing three times for 10 min in PBS supplemented with 0.2% Triton X-100 (PBST) at RT, the preparation was incubated with primary antibodies diluted in PBST overnight at 4°C, washed three times for 10 min in PBST at RT, incubated with secondary antibodies diluted in PBST for 1–2 h at RT, and washed two times with PBST for 10 min at RT. Confocal images were acquired the same day; otherwise, preparations were postfixed.

The following antibodies and dilutions were used: guinea pig anti-DCAF12 GP11, 1:20,000; guinea pig anti-DCAF12 GP12, 1:20,000; rabbit anti-Cul4, 1:1,000 (Lin et al., 2009; cat. no. Cul4, RRID: AB_2568621); mouse anti-Lamin-C, 1:250 (Developmental Studies Hybridoma Bank [DSHB]; cat. no. lc28.26, RRID: AB_528339); mouse anti-CSP, 1:250 (DSHB; cat. no. DCSP-1 [ab49], RRID: AB_2307340); rabbit anti-Syt1, 1:500 (Littleton et al., 1993; cat. no. Syt1, RRID: AB_2568644); mouse anti-Brp, 1:500 (DSHB; cat. no. nc82, RRID: AB_2314866); mouse anti-GluRIIA, 1:500 (DSHB; cat. no. 8B4D2 [MH2B], RRID: AB_528269);

mouse anti-discs large (DLG), 1:5,000 (DSHB; cat. no. 4F3, RRID: AB_528203); rabbit anti-vGlut, 1:10,000 (Aaron DiAntonio); rabbit anti-GluRIIB, 1:500 (Marrus et al., 2004; cat. no. GluRIIB, RRID: AB_2568753); rabbit anti-GluRIIC, 1:5,000 (Aaron DiAntonio); rabbit anti-GluRIID, 1:2,000 (Qin et al., 2005; cat. no. GluRIID, RRID: AB_2569238); mouse anti-ubiquitin-conjugated protein, 1:5,000 (Enzo Life Sciences; cat. no. BML-PW8810, RRID: AB_10541840); mouse anti-FLAG, 1:500 (Sigma-Aldrich; cat. no. P2983, RRID: AB_439685); mouse anti-Myc, 1:250 (DSHB; cat. no. 9E 10, RRID, AB_2266850); mouse anti-Repo, 1:100 (DSHB; cat. no. 8D12 anti-Repo, RRID: AB_528448); mouse anti-Futsch, 1:1,000 (DSHB; cat. no. 22c10, RRID: AB_528403); rabbit anti-SMT3, 1:1,000 (Lehembre et al., 2000; cat. no. smt3, RRID: AB_2568554); rabbit anti-Lola, 1:1,000 (Giniger et al., 1994; cat. no. lola, RRID: AB_2567779); rabbit anti-pMAD, 1:1,000 (Carl-Henrik Heldin, Göteborg University, Göteborg, Sweden; cat. no. pMad, RRID: AB_2617125); rabbit anti-coilin, 1:1,000 (Liu et al., 2009; cat. no. coil, RRID: AB_2568646); anti-γ-tubulin (GTU-88), 1:1,000 (Sigma-Aldrich; cat. no. T6557, RRID: AB_477584); goat anti-HRP Cy3-conjugated, 1:250 (Jackson ImmunoResearch Labs; cat. no. 123-165-021, RRID: AB_2338959); goat anti-guinea pig Alexa Fluor 488–conjugated, 1:1,000 (Thermo Fisher Scientific; cat. no. A-11073, RRID: AB_2534117); donkey anti-mouse Alexa Fluor 488–conjugated IgG (H + L), 1:1,000 (for GluRIIA stainings; Jackson ImmunoResearch Labs; cat. no. 715-545-150); goat anti-rabbit Alexa Fluor 488–conjugated, 1:1,000 (Thermo Fisher Scientific; cat. no. A-11008, RRID: AB_143165); goat anti-mouse Alexa Fluor 488–conjugated, 1:1,000 (Thermo Fisher Scientific; cat. no. A-21121, RRID: AB_2535764); goat anti-HRP Alexa Fluor 647–conjugated, 1:250 (Jackson ImmunoResearch Labs; cat. no. 123–605-021, RRID: AB_2338967). DNA was stained with DAPI (Thermo Fisher Scientific; cat. no. D3571, RRID: AB 2307445) at 1 µg/ml in PBST (pH 7.3) for 5 min at RT and washed two times for 10 min with PBS.

Stained preparations were imaged in PBS (pH 7.3) at RT with an Olympus microscope BX50WI equipped with a 60× water-immersion objective (LUMPLFL; N.A., 0.9). Images were acquired using a confocal laser scanner (Olympus FluoView300) using a multiargon (630), green HeNe (430), and/or a red HeNe (630) laser and BA 510, BA 530, BA 660, and/or BA 605 filters. Optical sections in the vertical axis were acquired in 1-µm intervals using Fluoview300 software. Acquired images were saved as raw data (TIFF files) in FluoView format. Display images were saved as 8-bit RGB TIFF files. Images were analyzed offline using ImageJ software (FIJI; National Institutes of Health). Fluorescence intensity measurements were performed on nondeconvoled z-stack images or single optical sections. Gamma adjustments were not performed. For publication, figures of images and data were compiled and prepared with Photoshop CC (Adobe). Contrast and intensity of images was minimally adjusted. Images were cropped, if necessary.

For quantification of fluorescence signals, control and mutant larvae were dissected in the same dish such that fixation and antibody incubation were performed identically. All samples were imaged with the same laser settings. Fluorescence intensity per area was determined from a region of interest encompassing single synaptic boutons or GluR clusters by using ImageJ Software.

To assess muscle size, muscle length and width were measured using ImageJ. Muscle surface area for muscles 6 and 7 was approximated by calculating the surface area of a cylinder. Bouton number was normalized to muscle surface area. For the analysis of ubiquitinated foci, the total number of distinct and bright FK2-positive puncta at the NMJ (both presynaptic and postsynaptic regions) were counted and normalized to NMJ length. The total number of FK2 puncta in nuclei were assessed by using the automatic nuclei counter ImageJ plug-in, ITCN (Image-based tool for counting nuclei).

Electrophysiology

Intracellular whole-cell recordings with a single microelectrode filled with 3 M KCl (20–40 MΩ) were made from muscle 6 (abdominal segment A3) of third-instar larvae in HL3 (70 mM NaCl, 5 mM KCl, 10 mM MgCl$_2$, 115 mM sucrose, 5 mM trehalose, 10 mM NaHCO$_3$, and 5 mM Hepes) supplemented with 0.6 mM Ca^{2+} unless otherwise specified. Recordings examining synaptic homeostasis used HL3 solution containing 4 mM MgCl$_2$. mEPPs were continuously recorded for 1 min, and the first 30 events were used to calculate average mEPP amplitudes. To elicit EPPs, the segmental nerve was stimulated through a glass capillary electrode (internal diameter, 10 µm) for 0.3 ms at 2 times the stimulus amplitude required for a threshold response. 15 EPPs were acquired at 0.1 Hz per larvae for analysis. Voltage signals were amplified with an Axoclamp 2B amplifier (Axon Instruments), filtered at 1 kHz, and digitized at 5 kHz directly to disk with a DigiData 1200 interface and pClamp 8.0 software (Axon Instruments). Evoked EPPs were analyzed using ClampFit 10.2 software (Molecular Devices), and spontaneous mEPPs were analyzed using Mini Analysis 6.0.0.7 (Synaptosoft). All experiments were performed at RT (20–22°C).

Data were collected from animals with resting membrane potentials less than –60 mV, and recording data were discarded when the resting membrane potential shifted >5 mV during the course of an experiment. Only one muscle per larvae was recorded in each individual experiment. For the baseline synaptic transmission data, animals with input resistances >4 MOhm were used. For neuronal rescue experiments, animals with input resistances >3 MOhm were used. Quantal content of evoked release was estimated by calculating the ratio of EPP/mEPP amplitudes and correcting for nonlinear summation using a reverse potential of 0 mV (Martin, 1955; Chang et al., 1994).

Western blot analysis

Third-instar larval brains were dissected in HL3, transferred to 2× Laemmli buffer (120 mM Tris HCl, pH 6.8, 4% SDS, 200 mM DTT, and 0.02% bromophenol blue), homogenized, boiled for 3 min, and centrifuged for 1 min. The soluble fraction was recovered, and ~1 brain equivalent was used for SDS-PAGE run at 80 V (Mini-Protean Cell; BioRad). Separated proteins were blotted onto nitrocellulose membranes at 20 V for 6 min using an iBlot system (Invitrogen). After transfer, the blot was blocked for 30 min using 5% nonfat dry milk or 2% BSA in 0.2% PBS Tween-20, pH 7.3. Blots were incubated with primary antibodies overnight at 4°C and HRP-conjugated secondary antibodies for 2 h at 4°C. To normalize for protein loading, blots were stripped (no. 21059;

Thermo Fisher Scientific) for 15 min at RT and immunoblotted for housekeeping proteins. Blots were imaged using a Bio-Rad Western Clarity ECL kit and ChemiDoc XRS imaging system. Protein band intensities were quantified via densitometry analysis with Quantity One software (Bio-Rad). Antibodies were diluted in PBS containing 0.2% Tween-20 as follows: anti-DCAF12, 1:20,000 (GP12); mouse anti-GFP, 1:500 (JL-8; Clontech; cat. no. 632380); mouse anti-V5, 1:1,000 (Thermo Fisher Scientific; cat. no. R960-25, RRID: AB_2556564); goat anti-GAPDH, 1:3,000 (Novus; cat. no. NB300-320, RRID: AB_10001796); mouse anti-β-tubulin, 1:1,000 (DSHB; cat. no. E7, RRID: AB_528499); goat anti-guinea pig HRP-conjugated 1:5,000 (Santa Cruz Biotechnology; cat. no. sc-2438, RRID: AB_650492); goat anti-mouse IgG HRP-conjugated 1:5,000 (Thermo Fisher Scientific; cat. no. 32430, RRID: AB_1185566).

GFP-trap assay

To generate N-terminal–tagged EGFP-DDB1, EGFP was cloned into a pMT/V5-His-C vector using XbaI and KpnI restriction sites (pMT/V5-EGFP). DDB1/piccolo cDNA was then PCR amplified using primers containing a KpnI (5′-TAGGTACCTCGCATCACTAC GTGGTGACGG-3′) or SpeI site (5′-TAACTAGTTCAATGCATGCG CGTGAGGTCCTCG-3′). The PCR products were cut with KpnI or SpeI and cloned in frame to EGFP of the pMT-EGFP vector. A stop codon after DDB1 precluded expression of downstream sequence including the C-terminal V5 and 6xHis-tags of the original pMT/V5-His-C vector. To generate N-terminal V5-tagged DCAF12, DCAF12 cDNA (DGRC) was PCR amplified using primers containing a KpnI (underlined) followed by a V5 tag (italic, 5′-TAGGTACCATGGGTAAGCCTATCCCTAACCCTCTCCTCGGTCTC GATTCTACGTTCAACGGGATGGTGAGAACCATCCGC-3′) or a NotI (underlined) site (5′-TAGCGGCCGCCTATTGCCAAACGCCCGCATA GTTGCCC-3′). The PCR product was cut with KpnI and NotI and cloned into a pMT/V5-His-C vector. A stop codon after DCAF12 precluded expression of the downstream V5 and 6x His-tags of the original vector.

Drosophila S2 cells were transfected with 2 µg total plasmid DNA using Amaxa Nucleofector 2b (Lonza). Expression of EGFP, V5-DCAF12, or EGFP-DDB1 was induced from the metallothionein promoter with 1.5 mM CuSO$_4$. After 24 h, proteins were extracted by lysing cells in 0.5 ml of cell lysis buffer (CLB; 50 mM Tris, pH 7.2, 125 mM NaCl, 1 mM EGTA, 1 mM DTT, 0.5% Triton X-100, 0.1 mM PMSF, and 10 µg/ml soy bean trypsin inhibitor). Extracts were clarified by centrifugation and diluted to 2–5 mg/ml in CLB. For GFP pull-downs (Rothbauer et al., 2008), purified GFP-binding protein (GFP-BP) was cross-linked to protein A–coupled Sepharose using dimethylpimelimidate. GFP-BP cross-linked beads were washed three times with 1.5 ml of cell lysis buffer and incubated with the protein extract for 45 min at 4°, washed three times with CLB, and resuspended in Laemmli sample buffer.

DCAF12-Cul4 coimmunoprecipitation

Protein A-G Plus agarose beads (sc-2003; Santa Cruz Biotechnology) were incubated with 4 µg mouse anti-Flag M2 (Sigma-Aldrich) on a rotator for 2 h at 4°C. 0.5 ml of fly heads was homogenized in 1 ml of IP buffer containing 1% Triton X-100, 25 mM Tris-HCl, pH 8.0, 150 mM NaCl, and the Complete Mini protease inhibitor cocktail (Sigma-Aldrich). After homogenization, the cell lysate was cleared of debris by centrifugation at 14,000 rpm for 10 min at 4°C. The cleared supernatant was then incubated with the Flag beads for 2 h on a rotator at 4°C. Agarose beads were spun down with a tabletop centrifuge at 2,000 rpm, and the supernatant was removed and stored. The beads were washed three times for 1 min with 100 µl of IP buffer via repeated resuspension and centrifugation at 2,000 rpm. Beads were resuspended in 2× Laemmli buffer, boiled for 3 min, and centrifuged for 1 min. The supernatant of precipitated proteins was used for SDS-PAGE and Western blot analysis.

Electron microscopy

Dissected larvae were fixed in Trump's fixative (1% paraformaldehyde, 3% glutaraldehyde, 100 mM cacodylate buffer [CB], pH 7.2, 2 mM sucrose, and 0.5 mM EGTA) for 1 to 2 h at RT and then overnight at 4°C. After washing in CB containing 264 mM sucrose (three times for 10 min), the tissue was postfixed with 2% OsO4 in CB for 1 h at RT, dehydrated in a series of ethanol dilutions (50%, 70%, 95%, and 100%) followed by propylene oxide, and embedded in Epon/Araldite. Serial cross sections were poststained with 4% uranyl acetate and lead citrate. Images were obtained on a JEOL 1200EX with an AMT XR80M-B camera running AMT software. For publication, figures were compiled and prepared with Photoshop CC. Contrast and intensity of images was minimally adjusted. Images were cropped, if needed.

Larval locomotion assay

Wandering third-instar larvae grown at 23°C were selected, washed gently with distilled water, and transferred with a paintbrush to the center of a 100 × 15-mm grape juice agar plate. Grape juice agar plates were made with Welch's 100% grape juice, distilled water, bacteriological agar, glacial acetic acid, and ethanol (Beverly Clendening, Hofstra University, Hempstead, NY). Larvae were recorded for 3 min, and the total distance traveled by each larva was calculated by scanning individual larval traces, which were manually drawn on the plate lid. Track length was measured with ImageJ software.

Data and statistical analysis

Data from at least three independent animals or experimental trials were used for statistical analysis. Data are represented as means, and error bars represent SEM. Gaussian distributions of data were assessed using a D'Agostino and Pearson omnibus or Shapiro–Wilk normality test. Statistical significance was assessed by either a two-tailed t test, Mann–Whitney, or one-way ANOVA (Kruskal–Wallis for nonparametric data) test with appropriate post hoc tests using Prism software (Graphpad Software).

Online supplemental material

Fig. S1 shows the subcellular localization of DCAF12 in larval neurons, glia, and muscles. Fig. S2 depicts structural effects and changes in synaptic GluR levels at dcaf12 mutant NMJs. Fig. S3 shows the electrophysiological properties of transmitter release and Mg^{2+} dependence of evoked release at dcaf12 mutant NMJs. Fig. S4 shows the subcellular localization of DCAF12 following presynaptic expression of DCAF12 or ΔNLS-DCAF12, the effects

of presynaptic and postsynaptic expression of DCAF12 or ΔN-LS-DCAF12 on electrophysiological properties of *dcaf12* mutant NMJs, and vGlut expression levels in controls and dcaf12 mutants. Fig. S5 shows effects of DCAF12 mutations on synaptic homeostasis and absolute values of the normalized data shown in Fig. 9, J–M.

References

Abbott, L.F., and W.G. Regehr. 2004. Synaptic computation. *Nature.* 431:796–803. https://doi.org/10.1038/nature03010

Angers, S., T. Li, X. Yi, M.J. MacCoss, R.T. Moon, and N. Zheng. 2006. Molecular architecture and assembly of the DDB1-CUL4A ubiquitin ligase machinery. *Nature.* 443:590–593.

Brand, A.H., and N. Perrimon. 1993. Targeted gene expression as a means of altering cell fates and generating dominant phenotypes. *Development.* 118:401–415.

Brusich, D.J., A.M. Spring, and C.A. Frank. 2015. A single-cross, RNA interference-based genetic tool for examining the long-term maintenance of homeostatic plasticity. *Front. Cell. Neurosci.* 9:107. https://doi.org/10.3389/fncel.2015.00107

Chang, H., S. Ciani, and Y. Kidokoro. 1994. Ion permeation properties of the glutamate receptor channel in cultured embryonic Drosophila myotubes. *J. Physiol.* 476:1–16.

Chen, C.Y., M.S. Tsai, C.Y. Lin, I.S. Yu, Y.T. Chen, S.R. Lin, L.W. Juan, Y.T. Chen, H.M. Hsu, L.J. Lee, and S.W. Lin. 2012. Rescue of the genetically engineered Cul4b mutant mouse as a potential model for human X-linked mental retardation. *Hum. Mol. Genet.* 21:4270–4285. https://doi.org/10.1093/hmg/dds261

Chen, Y.A., Y.J. Peng, M.C. Hu, J.J. Huang, Y.C. Chien, J.T. Wu, T.Y. Chen, and C.Y. Tang. 2015. The Cullin 4A/B-DDB1-Cereblon E3 ubiquitin ligase complex mediates the degradation of CLC-1 chloride channels. *Sci. Rep.* 5:10667. https://doi.org/10.1038/srep10667

Cline, H. 2003. Synaptic plasticity: Importance of proteasome-mediated protein turnover. *Curr. Biol.* 13:R514–R516. https://doi.org/10.1016/S0960-9822(03)00443-3

Daniels, R.W., C.A. Collins, M.V. Gelfand, J. Dant, E.S. Brooks, D.E. Krantz, and A. DiAntonio. 2004. Increased expression of the Drosophila vesicular glutamate transporter leads to excess glutamate release and a compensatory decrease in quantal content. *J. Neurosci.* 24:10466–10474. https://doi.org/10.1523/JNEUROSCI.3001-04.2004

Davis, G.W. 2006. Homeostatic control of neural activity: From phenomenology to molecular design. *Annu. Rev. Neurosci.* 29:307–323. https://doi.org/10.1146/annurev.neuro.28.061604.135751

Davis, G.W., and M. Müller. 2015. Homeostatic control of presynaptic neurotransmitter release. *Annu. Rev. Physiol.* 77:251–270. https://doi.org/10.1146/annurev-physiol-021014-071740

Deivasigamani, S., A. Basargekar, K. Shweta, P. Sonavane, G.S. Ratnaparkhi, and A. Ratnaparkhi. 2015. A presynaptic regulatory system acts trans-synaptically via Mon1 to regulate glutamate receptor levels in Drosophila. *Genetics.* 201:651–664. https://doi.org/10.1534/genetics.115.177402

Deshaies, R.J., and C.A. Joazeiro. 2009. RING domain E3 ubiquitin ligases. *Annu. Rev. Biochem.* 78:399–434. https://doi.org/10.1146/annurev.biochem.78.101807.093809

DiAntonio, A. 2006. Glutamate receptors at the Drosophila neuromuscular junction. *Int. Rev. Neurobiol.* 75:165–179. https://doi.org/10.1016/S0074-7742(06)75008-5

DiAntonio, A., S.A. Petersen, M. Heckmann, and C.S. Goodman. 1999. Glutamate receptor expression regulates quantal size and quantal content at the Drosophila neuromuscular junction. *J. Neurosci.* 19:3023–3032. https://doi.org/10.1523/JNEUROSCI.19-08-03023.1999

Dodge, F.A. Jr., and R. Rahamimoff. 1967. Co-operative action a calcium ions in transmitter release at the neuromuscular junction. *J. Physiol.* 193:419–432. https://doi.org/10.1113/jphysiol.1967.sp008367

Frank, C.A. 2014. Homeostatic plasticity at the Drosophila neuromuscular junction. *Neuropharmacology.* 78:63–74. https://doi.org/10.1016/j.neuropharm.2013.06.015

Fujimuro, M., H. Sawada, and H. Yokosawa. 1994. Production and characterization of monoclonal antibodies specific to multi-ubiquitin chains of polyubiquitinated proteins. *FEBS Lett.* 349:173–180. https://doi.org/10.1016/0014-5793(94)00647-4

Giniger, E., K. Tietje, L.Y. Jan, and Y.N. Jan. 1994. lola encodes a putative transcription factor required for axon growth and guidance in Drosophila. *Development.* 120:1385–1398.

Gratz, S.J., A.M. Cummings, J.N. Nguyen, D.C. Hamm, L.K. Donohue, M.M. Harrison, J. Wildonger, and K.M. O'Connor-Giles. 2013. Genome engineering of Drosophila with the CRISPR RNA-guided Cas9 nuclease. *Genetics.* 194:1029–1035. https://doi.org/10.1534/genetics.113.152710

Gratz, S.J., F.P. Ukken, C.D. Rubinstein, G. Thiede, L.K. Donohue, A.M. Cummings, and K.M. O'Connor-Giles. 2014. Highly specific and efficient CRISPR/Cas9-catalyzed homology-directed repair in Drosophila. *Genetics.* 196:961–971. https://doi.org/10.1534/genetics.113.160713

Guerrero-Santoro, J., M.G. Kapetanaki, C.L. Hsieh, I. Gorbachinsky, A.S. Levine, and V. Rapić-Otrin. 2008. The cullin 4B-based UV-damaged DNA-binding protein ligase binds to UV-damaged chromatin and ubiquitinates histone H2A. *Cancer Res.* 68:5014–5022. https://doi.org/10.1158/0008-5472.CAN-07-6162

Guo, X., G.T. Macleod, A. Wellington, F. Hu, S. Panchumarthi, M. Schoenfield, L. Marin, M.P. Charlton, H.L. Atwood, and K.E. Zinsmaier. 2005. The GTPase dMiro is required for axonal transport of mitochondria to Drosophila synapses. *Neuron.* 47:379–393. https://doi.org/10.1016/j.neuron.2005.06.027

Han, T.H., P. Dharkar, M.L. Mayer, and M. Serpe. 2015. Functional reconstitution of Drosophila melanogaster NMJ glutamate receptors. *Proc. Natl. Acad. Sci. USA.* 112:6182–6187. https://doi.org/10.1073/pnas.1500458112

Hannah, J., and P. Zhou. 2015. Distinct and overlapping functions of the cullin E3 ligase scaffolding proteins CUL4A and CUL4B. *Gene.* 573:33–45. https://doi.org/10.1016/j.gene.2015.08.064

He, Y.J., C.M. McCall, J. Hu, Y. Zeng, and Y. Xiong. 2006. DDB1 functions as a linker to recruit receptor WD40 proteins to CUL4-ROC1 ubiquitin ligases. *Genes Dev.* 20:2949–2954. https://doi.org/10.1101/gad.1483206

Hegde, A.N. 2017. Proteolysis, synaptic plasticity and memory. *Neurobiol. Learn. Mem.* 138:98–110. https://doi.org/10.1016/j.nlm.2016.09.003

Hegde, A.N., K. Inokuchi, W. Pei, A. Casadio, M. Ghirardi, D.G. Chain, K.C. Martin, E.R. Kandel, and J.H. Schwartz. 1997. Ubiquitin C-terminal hydrolase is an immediate-early gene essential for long-term facilitation in Aplysia. *Cell.* 89:115–126. https://doi.org/10.1016/S0092-8674(00)80188-9

Higa, L.A., and H. Zhang. 2007. Stealing the spotlight: CUL4-DDB1 ubiquitin ligase docks WD40-repeat proteins to destroy. *Cell Div.* 2:5. https://doi.org/10.1186/1747-1028-2-5

Higa, L.A., M. Wu, T. Ye, R. Kobayashi, H. Sun, and H. Zhang. 2006. CUL4-DDB1 ubiquitin ligase interacts with multiple WD40-repeat proteins and regulates histone methylation. *Nat. Cell Biol.* 8:1277–1283. https://doi.org/10.1038/ncb1490

Hubbard, J.I., S.F. Jones, and E.M. Landau. 1968. On the mechanism by which calcium and magnesium affect the spontaneous release of transmitter from mammalian motor nerve terminals. *J. Physiol.* 194:355–380. https://doi.org/10.1113/jphysiol.1968.sp008413

Hwangbo, D.S., B. Biteau, S. Rath, J. Kim, and H. Jasper. 2016. Control of apoptosis by Drosophila DCAF12. *Dev. Biol.* 413:50–59. https://doi.org/10.1016/j.ydbio.2016.03.003

Iovine, B., M.L. Iannella, and M.A. Bevilacqua. 2011. Damage-specific DNA binding protein 1 (DDB1): A protein with a wide range of functions. *Int. J. Biochem. Cell Biol.* 43:1664–1667. https://doi.org/10.1016/j.biocel.2011.09.001

Jackson, S., and Y. Xiong. 2009. CRL4s: The CUL4-RING E3 ubiquitin ligases. *Trends Biochem. Sci.* 34:562–570. https://doi.org/10.1016/j.tibs.2009.07.002

Jin, J., E.E. Arias, J. Chen, J.W. Harper, and J.C. Walter. 2006. A family of diverse Cul4-Ddb1-interacting proteins includes Cdt2, which is required for S phase destruction of the replication factor Cdt1. *Mol. Cell.* 23:709–721. https://doi.org/10.1016/j.molcel.2006.08.010

Jordán-Álvarez, S., W. Fouquet, S.J. Sigrist, and A. Acebes. 2012. Presynaptic PI3K activity triggers the formation of glutamate receptors at neuromuscular terminals of Drosophila. *J. Cell Sci.* 125:3621–3629. https://doi.org/10.1242/jcs.102806

Lehembre, F., P. Badenhorst, S. Müller, A. Travers, F. Schweisguth, and A. Dejean. 2000. Covalent modification of the transcriptional repressor tramtrack by the ubiquitin-related protein Smt3 in Drosophila flies. *Mol. Cell. Biol.* 20:1072–1082. https://doi.org/10.1128/MCB.20.3.1072-1082.2000

Lehman, N.L. 2009. The ubiquitin proteasome system in neuropathology. *Acta Neuropathol.* 118:329–347. https://doi.org/10.1007/s00401-009-0560-x

Li, S., X. Hu, S. Cui, and D. He. 2008. Novel centrosome protein, TCC52, is a cancer-testis antigen. *Cancer Sci.* 99:2274–2279. https://doi.org/10.1111/j.1349-7006.2008.00937.x

Lin, H.C., J.T. Wu, B.C. Tan, and C.T. Chien. 2009. Cul4 and DDB1 regulate Orc2 localization, BrdU incorporation and Dup stability during gene amplification in Drosophila follicle cells. *J. Cell Sci.* 122:2393–2401. https://doi.org/10.1242/jcs.042861

Littleton, J.T., H.J. Bellen, and M.S. Perin. 1993. Expression of synaptotagmin in Drosophila reveals transport and localization of synaptic vesicles to the synapse. *Development.* 118:1077–1088.

Liu, J.L., Z. Wu, Z. Nizami, S. Deryusheva, T.K. Rajendra, K.J. Beumer, H. Gao, A.G. Matera, D. Carroll, and J.G. Gall. 2009. Coilin is essential for Cajal body organization in Drosophila melanogaster. *Mol. Biol. Cell.* 20:1661–1670. https://doi.org/10.1091/mbc.e08-05-0525

Liu, J., J. Ye, X. Zou, Z. Xu, Y. Feng, X. Zou, Z. Chen, Y. Li, and Y. Cang. 2014. CRL4A(CRBN) E3 ubiquitin ligase restricts BK channel activity and prevents epileptogenesis. *Nat. Commun.* 5:3924. https://doi.org/10.1038/ncomms4924

Liu, W., A.F. Nichols, J.A. Graham, R. Dualan, A. Abbas, and S. Linn. 2000. Nuclear transport of human DDB protein induced by ultraviolet light. *J. Biol. Chem.* 275:21429–21434. https://doi.org/10.1074/jbc.M000961200

Lu, A., and S.R. Pfeffer. 2014. A CULLINary ride across the secretory pathway: More than just secretion. *Trends Cell Biol.* 24:389–399. https://doi.org/10.1016/j.tcb.2014.02.001

Mabb, A.M., and M.D. Ehlers. 2010. Ubiquitination in postsynaptic function and plasticity. *Annu. Rev. Cell Dev. Biol.* 26:179–210. https://doi.org/10.1146/annurev-cellbio-100109-104129

Marrus, S.B., and A. DiAntonio. 2004. Preferential localization of glutamate receptors opposite sites of high presynaptic release. *Curr. Biol.* 14:924–931. https://doi.org/10.1016/j.cub.2004.05.047

Marrus, S.B., S.L. Portman, M.J. Allen, K.G. Moffat, and A. DiAntonio. 2004. Differential localization of glutamate receptor subunits at the Drosophila neuromuscular junction. *J. Neurosci.* 24:1406–1415. https://doi.org/10.1523/JNEUROSCI.1575-03.2004

Martin, A.R. 1955. A further study of the statistical composition on the end-plate potential. *J. Physiol.* 130:114–122. https://doi.org/10.1113/jphysiol.1955.sp005397

Nakagawa, T., and Y. Xiong. 2011. X-linked mental retardation gene CUL4B targets ubiquitylation of H3K4 methyltransferase component WDR5 and regulates neuronal gene expression. *Mol. Cell.* 43:381–391. https://doi.org/10.1016/j.molcel.2011.05.033

Neves, G., S.F. Cooke, and T.V. Bliss. 2008. Synaptic plasticity, memory and the hippocampus: A neural network approach to causality. *Nat. Rev. Neurosci.* 9:65–75. https://doi.org/10.1038/nrn2303

Olma, M.H., M. Roy, T. Le Bihan, I. Sumara, S. Maerki, B. Larsen, M. Quadroni, M. Peter, M. Tyers, and L. Pintard. 2009. An interaction network of the mammalian COP9 signalosome identifies Dda1 as a core subunit of multiple Cul4-based E3 ligases. *J. Cell Sci.* 122:1035–1044. https://doi.org/10.1242/jcs.043539

Ozturk, N., S.J. VanVickle-Chavez, L. Akileswaran, R.N. Van Gelder, and A. Sancar. 2013. Ramshackle (Brwd3) promotes light-induced ubiquitylation of Drosophila Cryptochrome by DDB1-CUL4-ROC1 E3 ligase complex. *Proc. Natl. Acad. Sci. USA.* 110:4980–4985. https://doi.org/10.1073/pnas.1303234110

Parks, A.L., K.R. Cook, M. Belvin, N.A. Dompe, R. Fawcett, K. Huppert, L.R. Tan, C.G. Winter, K.P. Bogart, J.E. Deal, et al. 2004. Systematic generation of high-resolution deletion coverage of the Drosophila melanogaster genome. *Nat. Genet.* 36:288–292. https://doi.org/10.1038/ng1312

Petersen, S.A., R.D. Fetter, J.N. Noordermeer, C.S. Goodman, and A. DiAntonio. 1997. Genetic analysis of glutamate receptors in Drosophila reveals a retrograde signal regulating presynaptic transmitter release. *Neuron.* 19:1237–1248. https://doi.org/10.1016/S0896-6273(00)80415-8

Petroski, M.D., and R.J. Deshaies. 2005. Function and regulation of cullin-RING ubiquitin ligases. *Nat. Rev. Mol. Cell Biol.* 6:9–20. https://doi.org/10.1038/nrm1547

Pfaffl, M.W. 2001. A new mathematical model for relative quantification in real-time RT-PCR. *Nucleic Acids Res.* 29:e45. https://doi.org/10.1093/nar/29.9.e45

Qin, G., T. Schwarz, R.J. Kittel, A. Schmid, T.M. Rasse, D. Kappei, E. Ponimaskin, M. Heckmann, and S.J. Sigrist. 2005. Four different subunits are essential for expressing the synaptic glutamate receptor at neuromuscular junctions of Drosophila. *J. Neurosci.* 25:3209–3218. https://doi.org/10.1523/JNEUROSCI.4194-04.2005

Regehr, W.G. 2012. Short-term presynaptic plasticity. *Cold Spring Harb. Perspect. Biol.* 4:a005702. https://doi.org/10.1101/cshperspect.a005702

Rothbauer, U., K. Zolghadr, S. Muyldermans, A. Schepers, M.C. Cardoso, and H. Leonhardt. 2008. A versatile nanotrap for biochemical and functional studies with fluorescent fusion proteins. *Mol. Cell. Proteomics.* 7:282–289. https://doi.org/10.1074/mcp.M700342-MCP200

Saramäki, O.R., K.P. Porkka, R.L. Vessella, and T. Visakorpi. 2006. Genetic aberrations in prostate cancer by microarray analysis. *Int. J. Cancer.* 119:1322–1329. https://doi.org/10.1002/ijc.21976

Schaefer, H., and C. Rongo. 2006. KEL-8 is a substrate receptor for CUL3-dependent ubiquitin ligase that regulates synaptic glutamate receptor turnover. *Mol. Biol. Cell.* 17:1250–1260. https://doi.org/10.1091/mbc.e05-08-0794

Schmid, A., S. Hallermann, R.J. Kittel, O. Khorramshahi, A.M. Frölich, C. Quentin, T.M. Rasse, S. Mertel, M. Heckmann, and S.J. Sigrist. 2008. Activity-dependent site-specific changes of glutamate receptor composition in vivo. *Nat. Neurosci.* 11:659–666. https://doi.org/10.1038/nn.2122

Shiyanov, P., S.A. Hayes, M. Donepudi, A.F. Nichols, S. Linn, B.L. Slagle, and P. Raychaudhuri. 1999a. The naturally occurring mutants of DDB are impaired in stimulating nuclear import of the p125 subunit and E2F1-activated transcription. *Mol. Cell. Biol.* 19:4935–4943. https://doi.org/10.1128/MCB.19.7.4935

Shiyanov, P., A. Nag, and P. Raychaudhuri. 1999b. Cullin 4A associates with the UV-damaged DNA-binding protein DDB. *J. Biol. Chem.* 274:35309–35312. https://doi.org/10.1074/jbc.274.50.35309

Sjöström, P.J., E.A. Rancz, A. Roth, and M. Häusser. 2008. Dendritic excitability and synaptic plasticity. *Physiol. Rev.* 88:769–840. https://doi.org/10.1152/physrev.00016.2007

Song, T., S. Liang, J. Liu, T. Zhang, Y. Yin, C. Geng, S. Gao, Y. Feng, H. Xu, D. Guo, et al. 2018. CRL4 antagonizes SCFFbxo7-mediated turnover of cereblon and BK channel to regulate learning and memory. *PLoS Genet.* 14:e1007165. https://doi.org/10.1371/journal.pgen.1007165

Sulkowski, M., Y.J. Kim, and M. Serpe. 2014. Postsynaptic glutamate receptors regulate local BMP signaling at the Drosophila neuromuscular junction. *Development.* 141:436–447. https://doi.org/10.1242/dev.097758

Tai, H.C., and E.M. Schuman. 2008. Ubiquitin, the proteasome and protein degradation in neuronal function and dysfunction. *Nat. Rev. Neurosci.* 9:826–838. https://doi.org/10.1038/nrn2499

Tarpey, P.S., F.L. Raymond, S. O'Meara, S. Edkins, J. Teague, A. Butler, E. Dicks, C. Stevens, C. Tofts, T. Avis, et al. 2007. Mutations in CUL4B, which encodes a ubiquitin E3 ligase subunit, cause an X-linked mental retardation syndrome associated with aggressive outbursts, seizures, relative macrocephaly, central obesity, hypogonadism, pes cavus, and tremor. *Am. J. Hum. Genet.* 80:345–352. https://doi.org/10.1086/511134

Turrigiano, G. 2012. Homeostatic synaptic plasticity: Local and global mechanisms for stabilizing neuronal function. *Cold Spring Harb. Perspect. Biol.* 4:a005736. https://doi.org/10.1101/cshperspect.a005736

Wee, S., R.K. Geyer, T. Toda, and D.A. Wolf. 2005. CSN facilitates Cullin-RING ubiquitin ligase function by counteracting autocatalytic adapter instability. *Nat. Cell Biol.* 7:387–391. https://doi.org/10.1038/ncb1241

Wentzel, C., I. Delvendahl, S. Sydlik, O. Georgiev, and M. Müller. 2018. Dysbindin links presynaptic proteasome function to homeostatic recruitment of low release probability vesicles. *Nat. Commun.* 9:267. https://doi.org/10.1038/s41467-017-02494-0

Wu, J.T., H.C. Lin, Y.C. Hu, and C.T. Chien. 2005. Neddylation and deneddylation regulate Cul1 and Cul3 protein accumulation. *Nat. Cell Biol.* 7:1014–1020. https://doi.org/10.1038/ncb1301

Zou, Y., Q. Liu, B. Chen, X. Zhang, C. Guo, H. Zhou, J. Li, G. Gao, Y. Guo, C. Yan, et al. 2007. Mutation in CUL4B, which encodes a member of cullin-RING ubiquitin ligase complex, causes X-linked mental retardation. *Am. J. Hum. Genet.* 80:561–566. https://doi.org/10.1086/512489

Zou, Y., J. Mi, J. Cui, D. Lu, X. Zhang, C. Guo, G. Gao, Q. Liu, B. Chen, C. Shao, and Y. Gong. 2009. Characterization of nuclear localization signal in the N terminus of CUL4B and its essential role in cyclin E degradation and cell cycle progression. *J. Biol. Chem.* 284:33320–33332. https://doi.org/10.1074/jbc.M109.050427